Sensor Fault Estimation Using LPV Sliding Mode Observers with Erroneous Scheduling Parameters ⋆

Lejun Chen [a], Christopher Edwards [a], Halim Alwi [a]

[a] *College of Engineering, Mathematics and Physical Sciences, University of Exeter, Exeter, UK, EX4 4QF.*

Abstract

This paper proposes a linear parameter-varying sliding mode observer for the purpose of simultaneously estimating the system states and reconstructing sensor faults. Furthermore, some of the measured scheduling parameters are also assumed to be unreliable, and the corresponding values used in the observer are adapted to maintain the performance level of the observer. The adaptive algorithm is driven by the 'equivalent output error injection' signal associated with the reduced-order sliding motion. Sufficient conditions are given to ensure asymptotic stability of the state estimation error system, ensuring both the state estimation errors and the estimation errors associated with the scheduling parameters converge to zero. The efficacy of the scheme has been evaluated based upon an industrial high-fidelity aircraft benchmark scenario involving a simultaneous total loss of airspeed and angle of attack measurements.

Key words: Sliding mode observer; Linear parameter-varying; Fault detection and diagnosis.

1 Introduction

Sliding mode observer (SMO) techniques have been increasingly applied to solve Fault Detection and Diagnosis (FDD) problems, exploiting the equivalent injection concept (Alwi et al., 2011). In Edwards et al. (2000), an SMO was first employed to provide fault reconstruction in a linear system. Fault reconstruction, as a special case of the more general fault detection and isolation problem, is very useful in terms of developing active fault tolerant controllers (FTC) (Alwi and Edwards, 2008; Rotondo et al., 2015). A number of authors have extended typical adaptive observer structures and included sliding mode injection terms to improve parameter estimation robustness with respect to 'matched' uncertainty (Jiang et al., 2004; Efimov et al., 2016). More recently this work has been broadened to consider the presence of 'unmatched' uncertainty i.e. uncertainties or mismatches which affect the reduced order sliding dynamics (e.g. see Yan and Edwards (2008); de Loza et al. (2013); Alwi and Edwards (2014)). This is important because if the reduced-order sliding motion is affected by 'unmatched' uncertainty, the state estimation performance will be compromised, and the quality of the parameter estimation or fault reconstruction will be degraded.

To overcome these deficiencies, the work in Yan and Edwards (2008) employs an adaptive law within an SMO framework to recover fault reconstruction performance in the presence of significant 'unmatched' uncertainty. However, the adaptive algorithm proposed in Yan and Edwards (2008) requires knowledge of both the outputs and their derivatives. Also, to ensure asymptotic convergence of the error system, a nonlinear matrix inequality must be satisfied, which may be difficult to solve in practice for real engineering systems.

In recent years there has been significant interest in linear parameter-varying (LPV) system representations as a mechanism for extending the rich collection of linear based FDD/FTC methods to nonlinear systems (Marcos and Balas, 2004; Vanek et al., 2014, 2011; Varga and Ossmann, 2014; Ossmann and Varga, 2015; Hoffmann and Werner,

⋆ This paper was not presented at any IFAC meeting. Corresponding author C. Edwards.

Email addresses: Lejun.Chen@exeter.ac.uk (Lejun Chen), c.edwards@exeter.ac.uk (Christopher Edwards), h.alwi@exeter.ac.uk (Halim Alwi).

This paper has been accepted by Automatica *22 October 2018*

2015). However most of these existing FDD/FTC methods usually rely on accurate knowledge of the scheduling parameters. Some work has attempted to reduce the effect of inaccurate knowledge of the scheduling parameters during the synthesis process (Daafouz et al., 2008; Sato and Peaucelle, 2013; Chandra et al., 2016) by considering its effect as a plant/model mismatch to be mitigated by adopting a robust observer design. However, the mismatch in the scheduling parameters has to be relatively small to maintain FDD performance. In this paper, the problem is not predicated on the fact that the inaccuracy in the knowledge of the scheduling parameters is small. A generic adaptive LPV SMO scheme is proposed in this paper to simultaneously reconstruct the states and sensor faults whilst estimating accurately the value of the scheduling parameters. An adaptive algorithm is developed exploiting knowledge of the 'equivalent output error injection' signal. Assuming a Persistently Exciting (PE) plant trajectory, a sufficient condition is proposed to guarantee asymptotic stability of the error system. It is proved that the estimated scheduling parameters accurately approximate slowly varying scheduling parameters and 'unmatched' uncertainty in the reduced-order sliding mode is eliminated. Consequently, compared to Chandra et al. (2016), more accurate fault estimation can be achieved.

One application area in which LPV approaches have been extensively adopted is the field of aerospace. A challenge for upcoming and future aircraft is the extension of automatic Guidance Navigation and Control (GNC) functions to reduce pilot workload and to optimize the aircraft performance. One of the ways this can be achieved is to facilitate the automated handling of off-nominal so-called *abnormal* events. The aim of the EU-FP7 funded project RECONFIGURE (Reconfiguration of Control in Flight for Integral Global Upset Recovery) (Goupil et al., 2015) was to investigate and develop advanced GNC technologies to optimize the aircraft's status by automatically reconfiguring the aircraft to its optimal flight condition. Various specific scenarios have been identified by AIRBUS, and high fidelity benchmark simulations have been developed during the project to use for testing different FDD/FTC strategies. Descriptions of the benchmark model and the fault/failure scenarios are given in Goupil et al. (2015). This paper is motivated by one of the RECONFIGURE benchmark scenarios wherein measurements of both the airspeed and angle of attack are simultaneously totally lost (Goupil et al., 2015). The proposed scheme is applied to estimate both the calibrated airspeed (one of LPV scheduling parameters) and the angle of attack (one of output measurements). Once the sensor faults are well estimated, the corrupted measurements can be corrected before being used by the existing controller and the protection logic in an effort to ensure nominal performance is maintained (Alwi et al., 2012).

The remainder of the paper is structured as follows: the preliminaries are given in Section 2. In Section 3 the adaptive sliding mode observer scheme is developed for estimating the scheduling parameters and providing sensor fault reconstruction. The reaching and stability analysis of the sliding motion are given in Section 4 and Section 5, respectively. The fault estimation mechanism is discussed in Section 6. In Section 7, a systematic way of designing the observer is summarised. The RECONFIGURE benchmark problem developed by AIRBUS, which is used to demonstrate the efficacy of the scheme, is introduced in Section 8 and the design and industrial evaluation (Monte Carlo) campaign results are also given, whilst Section 9 gives some concluding remarks.

2 Problem Formulation and Preliminaries

In this section, an LPV sliding mode observer is proposed for a scenario in which the measured scheduling parameters are potentially corrupted. This distinguishes this paper from many of the earlier papers in the field of sliding mode based LPV FDD/FTC systems (Alwi and Edwards, 2014). Specifically, consider an LPV model of a plant with sensor faults:

$$\begin{aligned} \dot{x}_p(t) &= A_p(\rho)x_p(t) + B_p(\rho)u(t) \\ y_p(t) &= C_p x_p(t) + N_p f(t) \end{aligned} \tag{1}$$

where $A_p(\rho) \in \mathbb{R}^{n\times n}$, $B_p(\rho) \in \mathbb{R}^{n\times m}$, $C_p \in \mathbb{R}^{p\times n}$ and $N_p \in \mathbb{R}^{p\times q}$, where $q < p$. The matrix N_p is assumed to be full (column) rank and represents the sensor fault distribution matrix whose columns belong to the standard basis for $\mathbb{R}^p$. The scheduling parameter ρ is taken to belong to a polytope $\Theta \subset \mathbb{R}^r$. It is assumed that the signals $y_p(t)$ and $u(t)$ are available but the state vector $x_p(t)$ is unknown. The nominal scheduling parameter ρ is assumed to be measured but subject to possible faults. In (1), the signal $f(t)$ represents unknown faults (which are to be estimated).

Assumption 1 *The unknown faults $f(t)$ are norm bounded and $\|f(t)\| < \chi_2$, where χ_2 is a known positive scalar.*

In this paper, the parameter varying matrices are assumed to depend affinely on ρ, in particular,

$$A_p(\rho) = A_{p,0} + \sum_i^r \rho_i A_{p,i} \quad B_p(\rho) = B_{p,0} + \sum_i^r \rho_i B_{p,i} \tag{2}$$

where the scalar ρ_i represents the ith component of ρ. Based on (2) define aggregated matrices

$$\begin{aligned}\mathcal{A} &= \begin{bmatrix} A_{p,1} & A_{p,2} & \cdots & A_{p,r} \end{bmatrix} \in \mathbb{R}^{n\times nr} \\ \mathcal{B} &= \begin{bmatrix} B_{p,1} & B_{p,2} & \cdots & B_{p,r} \end{bmatrix} \in \mathbb{R}^{n\times mr}\end{aligned} \tag{3}$$

Since the columns of N_p are assumed to belong to the standard basis for $\mathbb{R}^p$, by permutating the outputs it is possible to obtain the representation

$$\begin{bmatrix} y_{p,1}(t) \\ y_{p,2}(t) \end{bmatrix} = \begin{bmatrix} C_{p,1} \\ C_{p,2} \end{bmatrix} x_p(t) + \begin{bmatrix} 0 \\ I_q \end{bmatrix} f(t) \tag{4}$$

where $C_{p,1} \in \mathbb{R}^{(p-q)\times n}$ and $C_{p,2} \in \mathbb{R}^{q\times n}$. In (4), $C_{p,1}$ is assumed to be full rank and $y_{p,2}(t)$ denotes the outputs which are potentially corrupted by faults whilst $y_{p,1}(t)$ are fault free. As in Alwi et al. (2011), define a new filter state $z_f(t) \in \mathbb{R}^q$ according to

$$\dot{z}_f(t) = -A_f z_f(t) + A_f y_{p,2}(t) \tag{5}$$

where $A_f \in \mathbb{R}^{q\times q}$ is a symmetric positive definite (s.p.d) matrix. Consider the augmented system from (1), (4) and (5), given by

$$\begin{aligned}\begin{bmatrix} \dot{x}_p(t) \\ \dot{z}_f(t) \end{bmatrix} &= \begin{bmatrix} A_p(\rho) & 0 \\ A_f C_{p,2} & -A_f \end{bmatrix} \begin{bmatrix} x_p(t) \\ z_f(t) \end{bmatrix} + \begin{bmatrix} B_p(\rho) \\ 0 \end{bmatrix} u(t) + \begin{bmatrix} 0 \\ A_f \end{bmatrix} f(t) \\ \begin{bmatrix} y_{p,1}(t) \\ z_f(t) \end{bmatrix} &= \begin{bmatrix} C_{p,1} & 0 \\ 0 & I_q \end{bmatrix} \begin{bmatrix} x_p(t) \\ z_f(t) \end{bmatrix}\end{aligned} \tag{6}$$

For the system in (6), define a coordinate transformation matrix

$$T_a = \mathrm{Diag}\{T_s, I_q\} \tag{7}$$

where $T_s \in \mathbb{R}^{n\times n}$ is any nonsingular matrix with the property that $C_{p,1}T_s^{-1} = \begin{bmatrix} 0 & I_{p-q} \end{bmatrix}$. Applying the coordinate transformation $x_p \mapsto x$ where $x = T_a x_p$ to the augmented system in (6), yields

$$\underbrace{\begin{bmatrix} \dot{x}(t) \\ \dot{z}_f(t) \end{bmatrix}}_{\dot{x}_a(t)} = \underbrace{\begin{bmatrix} T_s A_p(\rho) T_s^{-1} & 0 \\ A_f C_{p,2} T_s^{-1} & -A_f \end{bmatrix}}_{A(\rho)} \underbrace{\begin{bmatrix} x(t) \\ z_f(t) \end{bmatrix}}_{x_a(t)} + \underbrace{\begin{bmatrix} T_s B_p(\rho) \\ 0 \end{bmatrix}}_{B(\rho)} u(t) + \underbrace{\begin{bmatrix} 0 \\ A_f \end{bmatrix}}_{D} f(t) \tag{8}$$

where $y = \mathrm{col}(y_{p,1}, z_f) = Cx_a$, and $C = \begin{bmatrix} 0 & I_p \end{bmatrix}$.

The representation in (8) will now be used as the basis for the observer design. This is now a classical unknown input formulation in which $f(t)$ affects the states of the system and the outputs $y = Cx_a$. The structure of the proposes scheme is shown in Fig. 1.

3 Observer Formulation

The proposed sliding mode observer for the augmented system in (8) is

$$\dot{z}(t) = A(\hat{\rho})z(t) + B(\hat{\rho})u(t) + G_l e_y(t) + G_n \nu(t) \tag{9}$$

where $z(t) = \mathrm{col}(\hat{x}(t), \hat{z}_f(t))$ and $\hat{x}$ represents the estimate of x. In (9) the output estimation error is $e_y(t) = C(x_a(t) - z(t))$ and the nonlinear output error injection vector

$$\nu(t) = \begin{cases} k(t)\dfrac{e_y}{\|e_y\|} & \text{if } \ e_y \neq 0 \\ 0 & \text{otherwise} \end{cases} \tag{10}$$

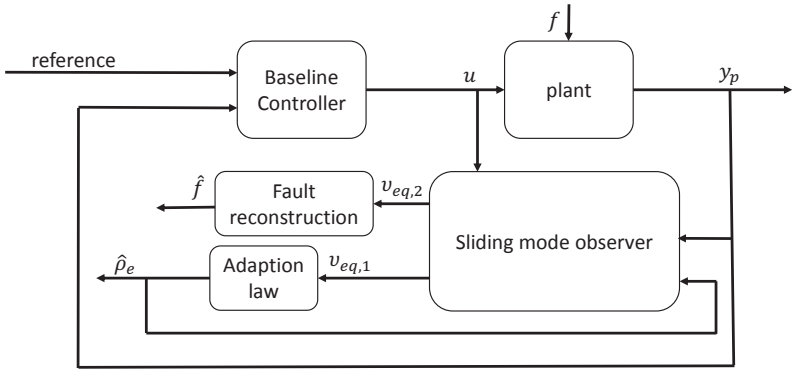

Fig. 1. The structure of the proposed scheme

where the modulation gain $k(t)$ is a positive scalar which will be defined later. In the observer structure in (9), if ρ was measured perfectly and known, ideally, $\hat{\rho}$ would be chosen equal to ρ. Here the aim is to create a scheme to adapt $\hat{\rho}$ so that $A(\hat{\rho}) = A(\rho)$ and $B(\hat{\rho}) = B(\rho)$ so as to avoid plant/observer model mismatches. A sufficient condition to ensure this is to force the mismatch $\rho - \hat{\rho}$ to zero. In practice the choice of scheduling parameters when creating the LPV model and the selection of an over-bounding polytope is important in term of minimising conservatism and promoting efficiency of the related observer design (Anstett et al., 2009).

Assumption 2 *The number of erroneous components of ρ is $h \leq r$ and the other components of $\hat{\rho}$ are identical to those in ρ.*

Define the scheduling parameter estimation error as

$$\tilde{\rho} := \rho - \hat{\rho} = \text{col}(\tilde{\rho}_1, \tilde{\rho}_2, \cdots, \tilde{\rho}_r) \tag{11}$$

then, when knowledge of the jth scheduling parameter ρ_j is exact (fault free), $\tilde{\rho}_j \equiv 0$. Define a matrix $U \in \mathbb{R}^{h \times r}$ to select the erroneous components of $\tilde{\rho}$, say $\tilde{\rho}_e \in \mathbb{R}^h$, so that

$$\tilde{\rho}_e = U\tilde{\rho} \tag{12}$$

Each row of U is taken from an rth order permutation matrix and so only one element per row is unity and the other terms are zeros. An example of calculating U will be given in Section 8.1. Correspondingly define

$$\rho_e = U\rho \quad \text{and} \quad \hat{\rho}_e = U\hat{\rho} \tag{13}$$

As in Alwi and Edwards (2014), the gain matrix $G_n \in \mathbb{R}^{(n+q)\times p}$ in (9) has the structure

$$G_n = \begin{bmatrix} -L \\ I_p \end{bmatrix} \tag{14}$$

where the parameter design matrix $L \in \mathbb{R}^{(n+q-p)\times p}$ is

$$L = \begin{bmatrix} L_1 & 0 \end{bmatrix} \tag{15}$$

and $L_1 \in \mathbb{R}^{(n+q-p)\times(p-q)}$. Here the other gain matrix

$$G_l = \begin{bmatrix} -\lambda L \\ \lambda I_p \end{bmatrix} \tag{16}$$

where λ is a positive design scalar (although other choices are possible (Alwi and Edwards, 2014)).

Define the state estimation error $e = x_a - z$, then from (8) and (9)

$$\dot{e} = A(\rho)e + \begin{bmatrix} T_s(A_p(\rho) - A_p(\hat{\rho}))T_s^{-1}\hat{x} + T_s(B_p(\rho) - B_p(\hat{\rho}))u \\ 0 \end{bmatrix} + Df - G_l e_y - G_n \nu \tag{17}$$

Define

$$\begin{aligned} A_e &= \mathcal{A}(U^T \otimes I_n) \in \mathbb{R}^{n \times nh} \\ B_e &= \mathcal{B}(U^T \otimes I_m) \in \mathbb{R}^{n \times mh} \end{aligned} \tag{18}$$

where $\otimes$ represents the Kronecker product and $\mathcal{A}$ and $\mathcal{B}$ are defined in (3). It is easy to verify from (12) that in the right hand side of (17)

$$T_s(A_p(\rho) - A_p(\hat{\rho}))T_s^{-1}\hat{x} = T_s A_e(\tilde{\rho}_e \otimes I_n)T_s^{-1}\hat{x} \tag{19}$$

and

$$T_s(B_p(\rho) - B_p(\hat{\rho}))u = T_s B_e(\tilde{\rho}_e \otimes I_m)u \tag{20}$$

By direct computation

$$(\tilde{\rho}_e \otimes I_n)T_s^{-1}\hat{x} = (I_h \otimes (T_s^{-1}\hat{x}))\tilde{\rho}_e \tag{21}$$

and

$$(\tilde{\rho}_e \otimes I_m)u = (I_h \otimes u)\tilde{\rho}_e \tag{22}$$

and therefore (17) can be conveniently written as

$$\dot{e} = A(\rho)e + \begin{bmatrix} T_s A_e(I_h \otimes (T_s^{-1}\hat{x})) + T_s B_e(I_h \otimes u) \\ 0 \end{bmatrix} \tilde{\rho}_e + Df - G_l e_y - G_n \nu \tag{23}$$

Assumption 3 *It is assumed*

$$rank(\begin{bmatrix} A_e & B_e \end{bmatrix}) = l < n \tag{24}$$

Using Assumption 3 in (23), the expression

$$A_e(I_h \otimes (T_s^{-1}\hat{x})) + B_e(I_h \otimes u) = H_p \phi(\hat{x}, u) \tag{25}$$

where $H_p \in \mathbb{R}^{n \times l}$ and in particular $\phi(\hat{x}, u) \in \mathbb{R}^{l \times h}$ is a known function.

Assumption 4 *The time varying matrix $\phi(\hat{x}, u)$ are bounded.*

Remark 1 *Equation (24) is a structural constraint on the matrices $\begin{bmatrix} A_e & B_e \end{bmatrix}$ and may be viewed as a limitation on the number of rows/channels in $A_p(\rho)$ and $B_p(\rho)$ which can depend on the erroneous scheduling variables ρ. It is of course a restriction, but an example of its application to a real engineering system will be given in Section 8.*

As a consequence of (25), system (23) be written as

$$\dot{e} = A(\rho)e + \begin{bmatrix} T_s H_p \\ 0 \end{bmatrix} \phi(\hat{x}, u)\tilde{\rho}_e + Df - G_l e_y - G_n \nu \tag{26}$$

Suppose $e = \text{col}(e_1, e_y)$, where, $e_1 \in \mathbb{R}^{n+q-p}$. Note the last p states in e correspond to the output estimation e_y since $C = \begin{bmatrix} 0 & I \end{bmatrix}$. Then (26) can be rewritten in the form

$$\begin{bmatrix} \dot{e}_1 \\ \dot{e}_y \end{bmatrix} = \begin{bmatrix} A_{11}(\rho) & A_{12}(\rho) \\ A_{21}(\rho) & A_{22}(\rho) \end{bmatrix} \begin{bmatrix} e_1 \\ e_y \end{bmatrix} + \begin{bmatrix} H_1 \\ H_2 \end{bmatrix} \phi(\hat{x}, u)\tilde{\rho}_e + \begin{bmatrix} 0 \\ D_2 \end{bmatrix} f - \begin{bmatrix} G_{l1} \\ G_{l2} \end{bmatrix} e_y - \begin{bmatrix} -L \\ I_p \end{bmatrix} \nu \tag{27}$$

where $A_{11}(\rho) \in \mathbb{R}^{(n+q-p)\times(n+q-p)}$ and the fixed distribution matrix $D_2 \in \mathbb{R}^{p\times q}$ is given by

$$D_2 = \begin{bmatrix} 0 \\ A_f \end{bmatrix} \tag{28}$$

Based on the parameter L from (15) define another coordinate transformation $e \mapsto T_L e = \tilde{e}$, given by

$$T_L = \begin{bmatrix} I_{n+q-p} & L \\ 0 & I_p \end{bmatrix} \tag{29}$$

Then exploiting the fact that $LD_2 = 0$ (because of the structures of L and D_2 from (15) and (28)), in the new coordinates equation (27) becomes

$$\begin{bmatrix} \dot{\tilde{e}}_1 \\ \dot{e}_y \end{bmatrix} = \begin{bmatrix} \tilde{A}_{11}(\rho) & \tilde{A}_{12}(\rho) \\ \tilde{A}_{21}(\rho) & \tilde{A}_{22}(\rho) \end{bmatrix} \begin{bmatrix} \tilde{e}_1 \\ e_y \end{bmatrix} + \begin{bmatrix} \tilde{H}_1 \\ \tilde{H}_2 \end{bmatrix} \phi(\hat{x}, u)\tilde{\rho}_e + \begin{bmatrix} 0 \\ D_2 \end{bmatrix} f - \begin{bmatrix} 0 \\ \lambda I_p \end{bmatrix} e_y - \begin{bmatrix} 0 \\ I_p \end{bmatrix} \nu \tag{30}$$

where $\tilde{e} = \mathrm{col}(\tilde{e}_1, e_y)$ and $\tilde{e}_1 = e_1 + Le_y$. In these new coordinates, the varying matrix

$$\tilde{A}_{11}(\rho) = A_{11}(\rho) + LA_{21}(\rho) \tag{31}$$

In this paper, the design freedom L is selected to ensure $\tilde{A}_{11}(\rho)$ from (31) is quadratically stable with respect to a Lyapunov function $V(\tilde{e}_1) = \tilde{e}_1^T P_1 \tilde{e}_1$. These dynamics govern the sliding motion.

4 Reaching Analysis

In this section the state estimation error in (30) will be analysed to demonstrate a sliding motion takes place on $e_y = 0$ in finite time.

Assumption 5 *There exists a s.p.d matrix P_1 such that for all $\rho \in \Theta$*

$$P_1\tilde{A}_{11}(\rho) + \tilde{A}_{11}(\rho)^T P_1 + q_1 I < 0 \tag{32}$$

where the scalar $q_1 > 0$.

Remark 2 *Since $A_{11}(\rho)$ and $A_{21}(\rho)$ depend linearly on the scheduling parameters and $\rho \in \Theta$ where Θ is a polytope, to satisfy the requirement (32), it is sufficient to synthesise L at the 2^r vertices of Θ and knowledge of ρ is not required. Necessary conditions for (31) to be solvable can be obtained by examining the vertices of $\tilde{A}_{11}(\rho)$, and requires each $(A_{11,i}, A_{21,i})$ be detectable. It can be shown unobservable modes of $(A_{11,i}, A_{21,i})$ correspond to (open-loop) eigenvalue of A_i (Tan and Edwards, 2002), and so a sufficient condition is that at each vertex the system is open loop stable.*

Remark 3 *Using the variable change $Y = P_1 L$, inequality (32) can be posed as an LMI problem in terms of P_1 and Y at each vertex of Θ.*

Lemma 1 *If Assumption 5 holds then, for a sufficiently large λ in (16), the matrix $P = Diag\{P_1, I_p\}$ has the property that*

$$Q(\rho) = P\tilde{A}_0(\rho) + \tilde{A}_0(\rho)^T P < 0 \tag{33}$$

where

$$\tilde{A}_0(\rho) = \begin{bmatrix} \tilde{A}_{11}(\rho) & \tilde{A}_{12}(\rho) \\ \tilde{A}_{21}(\rho) & \tilde{A}_{22}(\rho) - \lambda I_p \end{bmatrix} \tag{34}$$

Proof It follows from (33) and (34) and the diagonal structure of P that

$$\begin{aligned} Q(\rho) &= \begin{bmatrix} P_1\tilde{A}_{11}(\rho)+\tilde{A}_{11}(\rho)^T P_1 & \tilde{A}_{21}(\rho)^T+P_1\tilde{A}_{12}(\rho) \\ * & \tilde{A}_{22}(\rho)^T+\tilde{A}_{22}(\rho)-2\lambda I_p \end{bmatrix} \\ &:= \begin{bmatrix} Q_{11}(\rho) & Q_{12}(\rho) \\ * & Q_{22}(\rho)-2\lambda I_p \end{bmatrix} \end{aligned} \tag{35}$$

Since by hypothesis (Assumption 5) $Q_{11}(\rho) < 0$, exploiting the Schur complement, $Q(\rho) < 0$ if and only if

$$2\lambda I_p - Q_{22}(\rho) + Q_{12}(\rho)^T Q_{11}(\rho)^{-1} Q_{12}(\rho) > 0 \tag{36}$$

So choosing (for a given $P_1 > 0$) the scalar λ such that

$$\lambda > \frac{1}{2}\lambda_{max}\big(Q_{22}(\rho) - Q_{12}(\rho)^T Q_{11}(\rho)^{-1} Q_{12}(\rho)\big) \tag{37}$$

ensures (33). In (37), λ_{max} denotes the maximum eigenvalue. ■

By design it is assumed that P_1, $\tilde{A}_{11}(\rho)$ and λ have been chosen so that in (35)

$$Q(\rho) < -Q_0 < 0 \tag{38}$$

where Q_0 is a fixed design matrix. Define, in the state estimation error space $\tilde{e} = \mathrm{col}(\tilde{e}_1, e_y)$, a sliding surface

$$\mathcal{S} = \{\tilde{e} \in \mathbb{R}^{n+q} : C\tilde{e}(t) = 0\} \tag{39}$$

Since Θ is bounded, and from equations (11) and (13) $\tilde{\rho}_e = \rho_e - \hat{\rho}_e$, it follows using the triangle inequality

$$\|\tilde{\rho}_e(t)\| \leq \|\rho_e(t)\| + \|\hat{\rho}_e(t)\| \leq \theta_{max} + \|\hat{\rho}_e(t)\| \tag{40}$$

where θ_{max} represents a known upper bound of $\|\rho_e\|$. Consequently

$$\|\phi(\hat{x}, u)\tilde{\rho}_e\| \leq \eta_1(\hat{x}, u, \hat{\rho}_e) \tag{41}$$

where

$$\eta_1(\hat{x}, u, \hat{\rho}_e) = \|\phi(\hat{x}, u)\|(\theta_{max} + \|\hat{\rho}_e\|) \tag{42}$$

Note although $\tilde{\rho}_e$ is unknown (because ρ_e is unknown), $\eta_1(\cdot)$ is known since $\hat{x}$, u are known (and $\hat{\rho}_e$ is known being the estimate of the scheduling parameter). Therefore whilst the left hand side of the inequality in (41) is unknown, the upper bound $\eta_1(\hat{x}, u, \hat{\rho}_e)$ is known. Also note that, prior to sliding, it is assumed that $\hat{\rho}_e(t) = \hat{\rho}_e(0)$ and no adaptation takes place. In the remainder of this section, for improved readability the dependence of the signal ϕ on $\hat{x}$ and u will be dropped. Equation (30) can be written as

$$\dot{\tilde{e}}(t) = \tilde{A}_0(\rho)\tilde{e}(t) + \underbrace{\begin{bmatrix} \tilde{H}_1 \\ \tilde{H}_2 \end{bmatrix}}_{\tilde{H}} \phi(\cdot)\tilde{\rho}_e(t) + \begin{bmatrix} 0 \\ D_2 \end{bmatrix} f(t) - \begin{bmatrix} 0 \\ I_p \end{bmatrix} \nu(t) \tag{43}$$

where $\tilde{A}_0(\rho)$ is defined in (34), and λ and the Lyapunov matrix P for $\tilde{A}_0(\rho)$ are obtained from Lemma 1. Exploiting the structure of P in Lemma 1 it follows

$$\tilde{e}^T(t) P \begin{bmatrix} 0 \\ I_p \end{bmatrix} \nu(t) = k(t)\|e_y(t)\| \tag{44}$$

and

$$\tilde{e}^T(t)PD_2f(t) = \tilde{e}_y^T(t)D_2f(t) \tag{45}$$

where $\nu(t)$ and $k(t)$ are from (10) and $\tilde{e} = \text{col}(\tilde{e}_1, e_y)$. The objective is to obtain an upper bound on the evolution of $\|\tilde{e}(t)\|$ (to use in the modulation gain $k(t)$ employed to induce sliding). If $k(t) > \|D_2\|\chi_2(t)$ where $\chi_2(t)$ is defined in Assumption 1 (i.e. larger than the worst case norm of the fault) then using the Lyapunov function $V(\tilde{e}) = \tilde{e}^T P\tilde{e}$, from (43), (44) and (45), it can be shown that

$$\dot{V}(t) \leq \tilde{e}(t)^T Q(\rho)\tilde{e}(t) + 2\tilde{e}(t)^T P\tilde{H}\phi(\cdot)\tilde{\rho}_e(t) \tag{46}$$

It follows from (46) that

$$\dot{V} \leq -(P^{\frac{1}{2}}\tilde{e})^T P^{-\frac{1}{2}}Q_0P^{-\frac{1}{2}}P^{\frac{1}{2}}\tilde{e} + 2(P^{\frac{1}{2}}\tilde{e})^T P^{\frac{1}{2}}\tilde{H}\phi\tilde{\rho}_e(\cdot) \leq -\lambda_{min}(P^{-\frac{1}{2}}Q_0P^{-\frac{1}{2}})V + 2\sqrt{V}\|P^{\frac{1}{2}}\tilde{H}\|\|\phi\tilde{\rho}_e(\cdot)\| \tag{47}$$

where Q_0 is defined in (38) and λ_{min} denotes the minimum eigenvalue. In (47) the signal $\|\phi\tilde{\rho}_e(\cdot)\|$ is unknown because $\tilde{\rho}_e$ is unknown. However the upper bound from (41) depending on $\eta_1(\hat{x}, u, \hat{\rho}_e)$ is available. Writing $\mathcal{V} = \sqrt{V}$ it follows directly from (47) that

$$2\mathcal{V}\dot{\mathcal{V}} \leq -\lambda_{min}(P^{-\frac{1}{2}}Q_0P^{-\frac{1}{2}})\mathcal{V}^2 + 2\mathcal{V}\|P^{\frac{1}{2}}\tilde{H}\|\eta_1(\hat{x}, u, \hat{\rho}_e) \tag{48}$$

or equivalently for $\tilde{e} \neq 0$

$$\dot{\mathcal{V}}(t) \leq -q_0\mathcal{V}(t) + \|P^{\frac{1}{2}}\tilde{H}\|\eta_1(\hat{x}, u, \hat{\rho}_e) \tag{49}$$

where

$$q_0 = \frac{1}{2}\lambda_{min}(P^{-\frac{1}{2}}Q_0P^{-\frac{1}{2}}) > 0 \tag{50}$$

Define the scalar $\chi(t)$ as the solution of

$$\dot{\chi}(t) = -q_0\chi(t) + \|P^{\frac{1}{2}}\tilde{H}\|\eta_1(\hat{x}, u, \hat{\rho}_e) \tag{51}$$

where $\chi(0) = 0$. Comparing the solution of (51) with (49) it follows

$$\mathcal{V}(t) \leq e^{-q_0t}\mathcal{V}(0) + \int_0^t e^{-q_0(t-s)}\|P^{\frac{1}{2}}\tilde{H}\|\eta_1(\hat{x}, u, \hat{\rho}_e)ds = e^{-q_0t}\mathcal{V}(0) + \chi(t) \tag{52}$$

Let χ_0 be a positive design scalar, then $\chi(t) + \chi_0 > \mathcal{V}(t)$ for $t \geq t_0$ where $t_0 = \min\{0, \frac{1}{q_0}\log(\mathcal{V}(0)/\chi_0)\}$. Define

$$\tilde{\chi}(t) := (\chi(t) + \chi_0)/\sqrt{\lambda_{min}(P)} \tag{53}$$

then since $\mathcal{V}(t) > \sqrt{\lambda_{min}(P)}\|\tilde{e}(t)\|$, $\tilde{\chi}(t) \geq \|\tilde{e}(t)\|$ for $t \geq t_0$.

Remark 4 *$\tilde{\chi}(t)$ is an available quantity (since $\chi(t)$ can be obtained from solving (51) where $\eta_1(\hat{x}, u, \hat{\rho}_e)$ is known) and represents an upper bound on $\|\tilde{e}(t)\|$ for all $t > t_0$.*

Let

$$a_{21} := \max_{\rho\in\Theta}\|\tilde{A}_{21}(\rho)\| \quad a_{22} := \max_{\rho\in\Theta}\|\tilde{A}_{22}(\rho) - \lambda I_p\| \tag{54}$$

Lemma 2 *If the modulation gain in (10) is chosen to satisfy*

$$k(t) \geq a_{21}\tilde{\chi}(t) + a_{22}\|e_y(t)\| + \|\tilde{H}_2\|\eta_1(\hat{x}, u, \hat{\rho}_e) + \|D_2\|\chi_2(t) + \eta \tag{55}$$

where χ_2 represents a bound on the fault from Assumption 1 and η is a positive scalar, a sliding motion takes place for all $t \geq t_s \geq t_0$ where t_s is the finite time at which sliding is established.

Proof Define $\tilde{V}(e_y) = \frac{1}{2}e_y^T e_y$ then it follows from the expression for $\dot{e}_y$ in (30) that for all $t \geq t_0$

$$\begin{aligned}\dot{\tilde{V}} &= e_y^T(\tilde{A}_{21}(\rho)\tilde{e}_1 + \tilde{A}_{22}(\rho)e_y - \lambda I_p e_y + \tilde{H}_2\phi\tilde{\rho}_e + D_2 f - \nu) \\ &\leq \|e_y\|(a_{21}\tilde{\chi} + a_{22}\|e_y\| + \|\tilde{H}_2\|\eta_1(\cdot) + \|D_2\|\chi_2 - k) \leq -\eta\|e_y\| = -\eta\sqrt{2\tilde{V}}\end{aligned}$$

This ensures sliding takes place in finite time (Utkin (1992); Shtessel et al. (2013)). ■

The next section analyses the sliding motion and the adaptation law for $\hat{\rho}_e(t)$.

5 Reduced Order Sliding Motion Analysis

During sliding on $\mathcal{S}$, $\dot{e}_y = e_y = 0$ (Utkin, 1992). Consequently from (30) the reduced order sliding motion is governed by

$$\begin{aligned}\dot{\tilde{e}}_1 &= \tilde{A}_{11}(\rho)\tilde{e}_1 + \tilde{H}_1\phi(\hat{x}, u)\tilde{\rho}_e \\ 0 &= \tilde{A}_{21}(\rho)\tilde{e}_1 + \tilde{H}_2\phi(\hat{x}, u)\tilde{\rho}_e + D_2 f - \nu_{eq}\end{aligned} \tag{56}$$

where the quantity ν_{eq} is the equivalent output error injection necessary to maintain sliding (Utkin, 1992). By exploiting the structure of D_2 in (28), the bottom equation of (56) (associated with $e_y = 0$) can be further sub-partitioned into two parts: terms that are not directly affected by the fault f and those which are. To create this sub-partition define

$$\tilde{A}_{21}(\rho) = \begin{bmatrix}\tilde{A}_{211}(\rho) \\ \tilde{A}_{212}(\rho)\end{bmatrix}, \nu_{eq} = \begin{bmatrix}\nu_{eq,1} \\ \nu_{eq,2}\end{bmatrix}, \tilde{H}_2 = \begin{bmatrix}\tilde{H}_{21} \\ \tilde{H}_{22}\end{bmatrix} \tag{57}$$

where $\tilde{A}_{211}(\rho) \in \mathbb{R}^{(p-q)\times(n-p+q)}$, $\tilde{H}_{21} \in \mathbb{R}^{(p-q)\times l}$ and $\nu_{eq,1} \in \mathbb{R}^{p-q}$, then from (56)

$$\begin{aligned}\dot{\tilde{e}}_1 &= \tilde{A}_{11}(\rho)\tilde{e}_1 + \tilde{H}_1\phi(\hat{x}, u)\tilde{\rho}_e \\ \nu_{eq,1} &= \tilde{A}_{211}(\rho)\tilde{e}_1 + \tilde{H}_{21}\phi(\hat{x}, u)\tilde{\rho}_e\end{aligned} \tag{58}$$

Note the system in (58) does not directly depend on the faults $f(t)$.

During sliding, an arbitrary close approximation to ν_{eq} can be obtained (see for example (Shtessel et al., 2013)) and so $\nu_{eq,1}$ in (58) is known. The objective is to devise an adaption scheme for the observer scheduling parameter vector $\hat{\rho}_e$ to force the estimation error $\tilde{\rho}_e \to 0$ (and consequently to ensure $\tilde{e}_1 \to 0$).

Remark 5 *Note that the adaptation scheme described in this paper can only be employed whilst sliding is taking place during which the equivalent injection concept is valid. Here it is assumed in the adaption process will only take place for $t > t_s$ where t_s is given from Lemma 2.*

Remark 6 *It is clear from (58) that errors in estimating the scheduling parameters resulting in $\tilde{\rho}_e \neq 0$, generates an 'unmatched' term.*

An adaptive law will now be developed to describe the evolution of $\hat{\rho}_e(t)$ driven by the equivalent injection component $\nu_{eq,1}$.

Lemma 3 *(Zhang, 2002) A bounded and piecewise continuous vector or matrix $\Omega(t)$ is Persistently Exciting (PE), if for all $t > 0$, there exists $T > 0$ and $\varepsilon > 0$, such that*

$$\int_t^{t+T} \Omega(\sigma)^T\Omega(\sigma)d\sigma \geq \varepsilon I \tag{59}$$

Furthermore under these conditions, if Γ is a s.p.d matrix, then the system

$$\dot{\omega} = -\Gamma\Omega(t)^T\Omega(t)\omega \tag{60}$$

is exponentially stable. □

Introduce a design matrix $S \in \mathbb{R}^{h\times(p-q)}$ subject to the following assumption being satisfied:

Assumption 6 *The signal $S\tilde{H}_{21}\phi(\hat{x},u)$ is PE*[1] *.*

Then from (58) the available output signal $S\nu_{eq,1}$ evolves according to

$$\begin{aligned}\dot{\tilde{e}}_1(t) &= \tilde{A}_{11}(\rho)\tilde{e}_1 + \tilde{H}_1\phi(\hat{x},u)\tilde{\rho}_e \\ S\nu_{eq,1} &= S\tilde{A}_{211}(\rho)\tilde{e}_1 + S\tilde{H}_{21}\phi(\hat{x},u)\tilde{\rho}_e\end{aligned} \tag{61}$$

Assumption 7 *The scheduling parameter $\rho(t)$ associated with the plant is smooth and slowly varying.*

Remark 7 *Assumption 7 is a common assumption in LPV papers (and is quite reasonable for the civil aircraft example discussed later in the paper since such a system is not typically subject to aggressive acrobatic maneuvers).*

The following adaptation algorithm is proposed for $\hat{\rho}_e$:

$$\dot{\hat{\rho}}_e = \Gamma(S\tilde{H}_{21}\phi(\hat{x},u))^T S\nu_{eq,1} \tag{62}$$

where $\Gamma \in \mathbb{R}^{h\times h}$ is a s.p.d design matrix.

Under Assumption 7, by substituting (62) into (61) and using (11)

$$\dot{\tilde{e}}_1 = \tilde{A}_{11}(\rho)\tilde{e}_1 + \tilde{H}_1\phi\tilde{\rho}_e \tag{63}$$

$$\dot{\tilde{\rho}}_e = -\Gamma(S\tilde{H}_{21}\phi)^T S\tilde{A}_{211}(\rho)\tilde{e}_1 - \Gamma(S\tilde{H}_{21}\phi)^T S\tilde{H}_{21}\phi\tilde{\rho}_e \tag{64}$$

The system in (63)-(64) is equivalent to the nonlinear interconnected system shown in Fig. 2, where Σ_1 and Σ_2 represent the systems in (63) and (64) respectively.

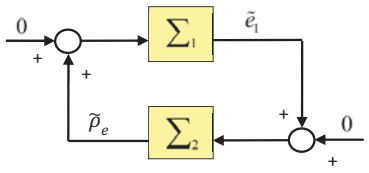

Fig. 2. Nonlinear interconnected error model

Define the time-varying matrices $\hat{A}(t)$ and $\hat{B}(t)$ as

$$\begin{aligned}\hat{A}(t) &= -\Gamma(S\tilde{H}_{21}\phi)^T S\tilde{H}_{21}\phi \\ \hat{B}(t) &= -\Gamma(S\tilde{H}_{21}\phi)^T S\tilde{A}_{211}(\rho)\end{aligned} \tag{65}$$

From Assumption 6, $S\tilde{H}_{21}\phi$ is PE, and therefore from Lemma 3, Σ_2 is zero input exponentially stable, i.e.

$$\dot{\tilde{\rho}}_e = \hat{A}(t)\tilde{\rho}_e \tag{66}$$

is exponentially stable. Consequently (see Theorem 4.11 in Khalil (2000)) the transition matrix $\Phi(t,t_0)$ associated with the solution to (66) satisfies

$$\|\Phi(t,t_0)\| < m_0 e^{-\lambda_0(t-t_0)} \tag{67}$$

for strictly positive scalars m_0 and λ_0. Define two scalars

$$p_2 = \frac{m_0^2}{\lambda_0} \tag{68}$$

[1] This implies the trajectory, and $u(t)$, must be sufficiently exciting.

and

$$b_0 \geq \|\hat{B}(t)\| = \|\Gamma(S\tilde{H}_{21}\phi)^T S\tilde{A}_{211}(\rho)\| \tag{69}$$

Note that the values of m_0 and λ_0 can be found since $\hat{A}(t)$ is known. A finite value for b_0 can be found since the boundedness of the right hand side of (69) follows from the boundedness of $\phi(\hat{x}, u)$ (Assumption 5).

Lemma 4 *For a scalar $\gamma_2 > \frac{p_2 b_0}{\sqrt{1-\epsilon_2}}$ where b_0 satisfies (69), p_2 is defined in (68) and $\epsilon_2 < 1$ is a small positive scalar, then there always exists a time-varying matrix $P_2(t) \in \mathbb{R}^{h\times h}$ such that*

$$0 < p_1 I_h \leq P_2(t) \leq p_2 I_h \tag{70}$$

for a finite positive scalar p_1 and

$$\dot{P}_2(t) + P_2(t)\hat{A}(t) + \hat{A}(t)^T P_2(t) + (1+\epsilon_2)I_h + \frac{1}{\gamma_2^2} P_2(t)\hat{B}(t)\hat{B}(t)^T P_2(t) < 0 \tag{71}$$

Proof Consider the time-varying matrix

$$P_2(t) = 2\int_t^\infty \Phi(s,t)^T \Phi(s,t) ds \tag{72}$$

where $\Phi(t, t_0)$ is the transition matrix associated with (66). From Theorem 4.12 in Khalil (2000), since (66) is exponentially stable there exist positive p_1 and p_2 such that (70) holds where a suitable choice for p_2 is given in (68). Furthermore, as argued in Theorem 4.12 in Khalil (2000), the matrix $P_2(t)$ satisfies (the Lyapunov equation)

$$\dot{P}_2(t) + P_2(t)\hat{A}(t) + \hat{A}(t)^T P_2(t) + 2I_h = 0 \tag{73}$$

Now consider the left hand side of the inequality in (71): if $\gamma_2 > \frac{p_2 b_0}{\sqrt{1-\epsilon_2}}$ where $b_0 \geq \|\hat{B}(t)\|$, then

$$\frac{1}{\gamma_2^2} P_2(t)\hat{B}(t)\hat{B}(t)^T P_2(t) < (1-\epsilon_2)I_h \tag{74}$$

and therefore

$$\dot{P}_2(t) + P_2(t)\hat{A}(t) + \hat{A}(t)^T P_2(t) + \frac{1}{\gamma_2^2} P_2(t)\hat{B}(t)\hat{B}(t)^T P_2(t) + (1+\epsilon_2)I_h \leq \dot{P}_2(t) + P_2(t)\hat{A}(t) + \hat{A}(t)^T P_2(t) + 2I_h \tag{75}$$

By construction $P_2(t)$ satisfies (73) and the right hand side of (75) zero. Therefore $P_2(t)$ from (72) satisfies inequality (71). ■

Since $\tilde{A}_{11}(\rho)$ is quadratically stable and $\phi(\hat{x}, u)$ is assumed to be bounded, there exist a positive scalar γ_1 and a fixed matrix $P_1 > 0$ such that

$$P_1\tilde{A}_{11}(\rho) + \tilde{A}_{11}(\rho)^T P_1 + \frac{1}{\gamma_1^2} P_1\tilde{H}_1\phi\phi^T\tilde{H}_1^T P_1 + (1+\epsilon_1)I < 0 \tag{76}$$

where ϵ_1 is a positive scalar.

Theorem 1 *Let γ_1 be chosen so there exists a P_1 that (76) holds, and suppose γ_2 satisfies the conditions of Lemma 4. Then if*

$$\gamma_1\gamma_2 < 1 \tag{77}$$

the nonlinear system in Fig. 2 is exponentially stable.

Proof As shown in Fig. 2, let the two interconnected systems $\Sigma_1 : \tilde{\rho}_e \mapsto \tilde{e}_1$ and $\Sigma_2 : \tilde{e}_1 \mapsto \tilde{\rho}_e$ be given by $(\tilde{A}_{11}(\rho), \tilde{H}_1\phi(t), I)$ and $(\hat{A}(t), \hat{B}(t), I)$ respectively. From Lemma 4 there exist a γ_2 and $p_1 I < P_2(t) \leq p_2 I$ such that

$$\dot{P}_2(t) + P_2(t)\hat{A}(t) + \hat{A}(t)^T P_2(t) + \epsilon_2 I + \frac{1}{\gamma_2^2} P_2(t)\hat{B}(t)\hat{B}(t)^T P_2(t) + I < 0 \tag{78}$$

Now for the system in Fig. 2 consider as a candidate Lyapunov function

$$V(t) = \frac{1}{\gamma_1^2}\tilde{e}_1^T P_1 \tilde{e}_1 + \tilde{\rho}_e^T P_2(t)\tilde{\rho}_e \tag{79}$$

which is positive definite w.r.t to $\tilde{e}_1$ and $\tilde{\rho}_e$ and radially unbounded. It follows

$$\dot{V}(t) = \frac{1}{\gamma_1^2}\big(\tilde{e}_1^T(P_1\tilde{A}_{11}(\rho) + \tilde{A}_{11}(\rho)^T P_1)\tilde{e}_1 + 2\tilde{e}_1^T P_1 \tilde{H}_1 \phi \tilde{\rho}_e\big) + \tilde{\rho}_e^T \dot{P}_2(t)\tilde{\rho}_e + \tilde{\rho}_e^T(P_2(t)\hat{A}(t) + \hat{A}(t)^T P_2(t))\tilde{\rho}_e + 2\tilde{\rho}_e^T P_2(t)\hat{B}(t)\tilde{e}_1 \tag{80}$$

and using Young's Inequality,

$$\begin{aligned}\dot{V}(t) \leq \frac{1}{\gamma_1^2}\big(\tilde{e}_1^T(P_1\tilde{A}_{11}(\rho) + \tilde{A}_{11}(\rho)^T P_1)\tilde{e}_1 + \frac{1}{\gamma_1^2}\tilde{e}_1^T P_1 \tilde{H}_1 \phi\phi^T \tilde{H}_1 P_1 \tilde{e}_1 + \gamma_1^2\|\tilde{\rho}_e\|^2\big) \\ + \tilde{\rho}_e^T \dot{P}_2(t)\tilde{\rho}_e + \tilde{\rho}_e^T(P_2(t)\hat{A}(t) + \hat{A}(t)^T P_2(t))\tilde{\rho}_e + \frac{1}{\gamma_2^2}\tilde{\rho}_e^T P_2(t)\hat{B}(t)\hat{B}(t)^T P_2\tilde{\rho}_e + \gamma_2^2\|\tilde{e}_1\|^2\end{aligned}$$

Then using (76) and (78), it follows from (81) that

$$\begin{aligned}\dot{V}(t) &\leq \frac{1}{\gamma_1^2}(\gamma_1^2\|\tilde{\rho}_e\|^2 - (1+\epsilon_1)\|\tilde{e}_1\|^2) + \gamma_2^2\|\tilde{e}_1\|^2 - (1+\epsilon_2)\|\tilde{\rho}_e\|^2 \\ &= \|\tilde{\rho}_e\|^2 - \frac{(1+\epsilon_1)}{\gamma_1^2}\|\tilde{e}_1\|^2 + \gamma_2^2\|\tilde{e}_1\|^2 - (1+\epsilon_2)\|\tilde{\rho}_e\|^2 \\ &= -\frac{1}{\gamma_1^2}\|\tilde{e}_1\|^2 + \gamma_2^2\|\tilde{e}_1\|^2 - \frac{\epsilon_1}{\gamma_1^2}\|\tilde{e}_1\| - \epsilon_2\|\tilde{\rho}_e\|^2 \\ &= (-\frac{1}{\gamma_1^2} + \gamma_2^2)\|\tilde{e}_1\|^2 - \frac{\epsilon_1}{\gamma_1^2}\|\tilde{e}_1\| - \epsilon_2\|\tilde{\rho}_e\|^2\end{aligned} \tag{81}$$

It is clear from (81) that if $\gamma_1\gamma_2 < 1$,

$$\dot{V}(t) \leq -\frac{\epsilon_1}{\gamma_1^2}\|\tilde{e}_1\| - \epsilon_2\|\tilde{\rho}_e\|^2 \tag{82}$$

and the system in Fig. 2 is asymptotically stable. ■

6 Fault Estimation

The previous section has provided a set of conditions under which the adaption scheme to estimate the corrupted scheduling parameters guarantee the reduced order sliding motion in (83) is asymptotically stable and $\tilde{e}_1(t) \to 0$ as $t \to \infty$. To develop the adaption law for $\hat{\rho}_e(t)$ in (62) the equivalent injection signal ν_{eq} from (83) was decomposed as $\text{col}(\nu_{eq,1}, \nu_{eq,2})$ and only $\nu_{eq,1} \in \mathbb{R}^{p-q}$ was used in the adaption law. By construction the adaption loop is independent of the faults. Since, as argued in Section 5, $\nu_{eq,2}$ is available in real time, an estimate of the fault $\hat{f}(t)$ will be created based on $\nu_{eq,2}$.

From (57) it follows the other component of ν_{eq}, namely $\nu_{eq,2} \in \mathbb{R}^q$, satisfies

$$\nu_{eq,2} = \tilde{A}_{212}(\rho)\tilde{e}_1 + \tilde{H}_{22}\phi(\hat{x}, u)\tilde{\rho}_e + A_f f \tag{83}$$

If the conditions in Section 5 are met then it follows $\tilde{e}_1(t) \to 0$ and $\tilde{\rho}_e(t) \to 0$ as $t \to \infty$ and it follows from (83) that $\nu_{eq,2} \to A_f f$. Therefore

$$\hat{f} := A_f^{-1}\nu_{eq,2} \tag{84}$$

represents a useful reconstruction of the fault after the convergence of $\tilde{\rho}_e(t)$ and and $\tilde{e}_1(t)$ to zero. Specifically, once sliding is established, if the conditions of Theorem 1 in Section 5 hold, $\hat{f}(t) \to f(t)$ as $t \to \infty$.

7 Design Summary and Notes on Tuning

An outline of the design method summarizing the developments in the previous section is as follows:

(1) Re-order the system states such that the sensors considered prone to faults are in the lower half of the output vector as given in (4).
(2) Augment the plant model from (1) with the filtered version of the sensors prone to faults to create the system in (6). This involves selection of the matrix A_f in (5) which governs the bandwidth of the filter.
(3) Change the coordinates of the augmented system using (7) so that the output distribution matrix C is as given in (8).
(4) Compute the perturbation matrix U from the indices of erroneous scheduling parameters and calculate A_e and B_e from (18). Then find H_p from (25) which identifies the rows in the system matrix associated with the erroneous scheduling variables. Consequently H_1 and H_2 can be calculated from (26) and (27).
(5) Using Remark 3, (32) becomes an LMI. Then compute the Lyapunov matrix P_1 and the gain L to satisfy (32).
(6) Once P_1 and L have been obtained from Step (5), λ can be selected from (37) and the observer gain G_l in (16) is completely specified.
(7) Once L has been obtained, the nonlinear gain G_n given in (14) is specified.
(8) Once P_1 and L have been obtained, first Q_0 can be selected from (38), then q_0 from (50).
(9) Create the observer in (9) using the scheduling parameters $\hat{\rho}$ constructed from (62). In (62), the design matrix Γ is selected to improve the exponential convergence rate and the gain S is chosen to adjust and ensure persistence of excitation.
(10) The modulation gain $k(t)$ must be chosen to satisfy (55). In (55), χ_2 is known and defined in Assumption 1, a_{21} and a_{22} are selected from (54), H_2 is known from Step (4), D_2 is from (28), $\tilde{\chi}(t)$ is from (53) where $\chi(t)$ is obtained by solving (51) (since q_0 in Step(8) and $\eta_1(\hat{x}, u, \hat{\rho}_e)$ are known).
(11) According to the stability analysis in Section 5, once the sliding motion occur, the adaptation process takes place and $\tilde{\rho}_e$ starts converging to zero. From equation (83), the reconstruction signal is defined as $\hat{f} := A_f^{-1}\nu_{eq,2}$ after the convergence of $\tilde{\rho}_e$.

8 RECONFIGURE Benchmark Problem

In this section, the proposed scheme will be applied to solve a RECONFIGURE benchmark problem. The RECONFIGURE benchmark developed by AIRBUS is based on a nonlinear highly representative model of a generic civil commercial aircraft. This aircraft model has been used within the EU funded RECONFIGURE project as the basis for all the scenarios and for testing different fault detection and fault tolerant control strategies. In this paper a benchmark scenario involving *the simultaneous total loss of the calibrated airspeed (VCAS) measurement and an angle of attack (AOA) measurement* sensor fault is considered. In the benchmark scenario, it is assumed the VCAS and AOA measurements are lost simultaneously and almost immediately. Once lost they are not recovered (Goupil et al., 2015). In this section, both preliminary design results based on a simplified LPV model and RECONFIGURE benchmark simulation results based on the industrial V&V (validation and verification) campaign will be shown, to demonstrate the design efficacy.

8.1 Preliminary design results

To improve the transparency of the design process, this section describes preliminary design and simulation results based on a simplified LPV model built via interpolation of multiple LTI models [2]. In this subsection, it is used for both design and initial testing.

The affine aircraft LPV model in the form of (1) is described Appendix A and the four scheduling parameters are

$$\rho = \begin{bmatrix} w(\text{t}) & \text{CG}(\%) & \text{VCAS(kt)} & h(\text{ft}) \end{bmatrix}^T \tag{85}$$

[2] LTI models associated with various flight conditions were provided by Airbus for the *design* of FDD/FTC schemes.

These represent the aircraft weight, the position of the centre of gravity, calibrated airspeed and altitude. *The RECONFIGURE benchmark is a civil aircraft, and so the assumption that the velocity VCAS is slowly varying is a reasonable one for this application.* In this paper, the ranges of the scheduling parameters are not provided due to industrial confidentiality restrictions, and all the scheduling parameters have been normalized to lie in the interval [0 1]. The state variables are

$$x_p = \begin{bmatrix} q & V_g & \alpha & \theta & Z_g \end{bmatrix}^T \tag{86}$$

and represent pitch rate, ground speed, angle of attack, pitch angle and altitude respectively. In this paper it is assumed only a subset of the states are measured. In particular, the variable V_g is not regarded as available. For the purpose of achieving the 'output canonical form' described earlier, the output variables are reordered as

$$y_p = \left[\begin{array}{ccc|c} q & \theta & Z_g & \alpha \end{array}\right]^T \tag{87}$$

The system input vector is given by $u = \begin{bmatrix} \delta_e & \delta_{stab} \end{bmatrix}^T$ where δ_e denotes the deflection of the elevators and δ_{stab} is the deflection of the horizontal stabilizer.

Since the third scheduling parameter VCAS is erroneous, from (12), $U = [0 \;\; 0 \;\; 1 \;\; 0]$ and $h = 1$. The matrices A_e and B_e formed from the coefficients associated with ρ_3 are

$$\begin{bmatrix} A_e & B_e \end{bmatrix} = \left[\begin{array}{ccccc|cc} -0.5247 & 0.0025 & -0.5898 & 0 & 0 & -0.6856 & -1.4287 \\ 0 & -0.0007 & 0.0216 & 0 & 0 & 0 & 0.0033 \\ -0.0137 & 0.0086 & -0.3832 & 0 & 0 & -0.0220 & -0.0493 \\ 0 & 0 & 0 & 0 & 0 & 0 & 0 \\ 0 & 0 & -0.1411 & 0.1411 & 0 & 0 & 0 \end{array}\right] \tag{88}$$

Clearly, $l = \text{rank}([A_e \;\; B_e]) = 4$ and Assumption 3 is verified. The matrix H_p from (26) can be selected as

$$H_p = \begin{bmatrix} 1 & 0 & 0 & 0 \\ 0 & 1 & 0 & 0 \\ 0 & 0 & 1 & 0 \\ 0 & 0 & 0 & 0 \\ 0 & 0 & 0 & 1 \end{bmatrix} \quad H_1 = \begin{bmatrix} 0 & -1 & 0 & 0 \\ 0 & 0 & -1 & 0 \end{bmatrix} \quad H_2 = \begin{bmatrix} 1 & 0 & 0 & 0 \\ 0 & 0 & 0 & 0 \\ 0 & 0 & 0 & 1 \\ 0 & 0 & 0 & 0 \end{bmatrix} \tag{89}$$

and relates to rows in which the scheduling parameter ρ_3 appears. Once H_p is defined, in this example, it can be shown that matrices H_1 and H_2 have the structures given above. As a consequence, from (25)

$$\phi(\hat{x}, u) = \begin{bmatrix} 1 & 0 & 0 & 0 & 0 \\ 0 & 1 & 0 & 0 & 0 \\ 0 & 0 & 1 & 0 & 0 \\ 0 & 0 & 0 & 0 & 1 \end{bmatrix} \begin{bmatrix} A_e & B_e \end{bmatrix} \begin{bmatrix} T_s^{-1}\hat{x} \\ u \end{bmatrix} \tag{90}$$

where T_s is known and satisfies $C_{p,1}T_s^{-1} = [0 \;\; I_{p-q}]$. The filter parameter A_f from (5) has been chosen as $A_f = 1$. After computing a suitable gain matrix L using YALMIP (Löfberg, 2004), the matrices $\tilde{A}_{11}(\rho)$, $\tilde{H}_1$ and $\tilde{H}_2$ can be established. In this example, the scalar γ_1 from (76) is 0.7433. In this design

$$S = \begin{bmatrix} 1 & 0 & 0 \end{bmatrix} \tag{91}$$

and $\lambda = 78$. Furthermore from (50), $q_0 = 0.0453$. From (62), the matrix $\Gamma = 16$ (which governs the convergence rate of the estimation error). Since ρ_3 has been normalized in the interval [0 1], in (41), $\theta_{max} = 1$ and hence $\eta_1 = \|\phi(\hat{x}, u)\|(1 + \|\hat{\rho}_e\|)$. This will be used to create $\tilde{\chi}(t)$ obtained from solving the differential equation (51).

In order to show the effectiveness of the preliminary design, one vertex of the polytope is selected as the testing point. The robust performance of the scheme will be subsequently demonstrated in Section 8.2 using the nonlinear RECONFIGURE benchmark. In this example, the pilot input, shown in Fig. 3(a), provides sufficient excitation for the adaptive scheme.

Simulation results involving the total loss of the VCAS and AOA signals are shown in Figs. 3-5. Here it is assumed the VCAS signal (the third scheduling parameter) is totally lost from the beginning of the simulation, whereas the AOA (output) measurement becomes faulty (and is assumed to be totally lost) after 10 sec which coincides with an AOA manoeuvre. The values of AOA in both the nominal and faulty cases are shown in Fig. 3(b).

The parameter $\tilde{\chi}(t)$ created from (51) and (53) is shown in Fig. 4(a). Figure 4(b) shows sliding occurs almost immediately whilst Fig. 4(c) shows the norm of the states of the estimation error $\|e_1\|$, which is vanishing since the unmatched uncertainties relating to $\tilde{\rho}_e$ are compensated for.

The error between the nominal VCAS measurement and its estimates (i.e. $\tilde{\rho}_e$), is shown in Fig. 5(a). Despite the fact VCAS measurement is totally lost from the beginning of the simulation, the estimation error $\tilde{\rho}_e$ rapidly converge to zero only once persistent excitation has been induced by the pilot from 5sec onwards (See Fig. 3(a)). The zero estimation errors for $\tilde{\rho}_e$ indicate that the observer has managed to provide a good reconstruction of the actual VCAS. The AOA fault reconstruction is shown in Fig. 5(b). It shows that the fault reconstruction signal can approximate the actual faults accurately after the convergence of VCAS.

8.2 RECONFIGURE benchmark simulation

The RECONFIGURE benchmark is a nonlinear highly representative model of a generic civil commercial aircraft which contains a baseline gain-scheduled controller, detailed actuator and sensor models, as well as angle of attack and speed protection components and measurement filters. The simulation model of RECONFIGURE is 'invisible' for design purposes and runs as a 'blackbox' in a LINUX environment. The flight control computer component is extracted in a Simulink model which includes the baseline LPV controller, and ways to 'plug in' FDD/FTC designs (Goupil et al., 2015).

During the industrial V&V campaign, both the VCAS and AOA measurements are assumed to be lost and almost immediately from the beginning of the simulation. The objective of the design is to maintain longitudinal *C-NZ* performance in the face of the total loss of VCAS and AOA for various operating conditions and deliberate validation activities.

In this section, one of the industrial *C-NZ* validation activities, the so-called 'NZLAW-05' maneuver is performed for the verification of GNC performance and is used for assessing robustness and performance of the design in the presence of a total loss of VCAS and AOA. Details of this maneuver will be discussed later. The efficacy of the proposed scheme during 'NZLAW-05' will be evaluated based on the accuracy of the fault estimation and longitudinal *C-NZ* performance. Once the LPV sliding mode observer has the capability of reconstructing VCAS and AOA faults, the reconstruction signals are used to 'correct' the corrupted VCAS and AOA measurements before they are used by the existing AIRBUS controller and protection logic. According to Alwi et al. (2012), only a small modification to the feedback loop is required to implement this approach and the observer can be designed independently of the controller. The idea in Alwi et al. (2012) results in a scheme with low computational load, as a result of retrofitting within the existing control system, and the nominal protected *C-NZ* performance is retained in the presence of VCAS and AOA faults. This is appealing especially for aerospace applications where strict certification rules apply. Details of the stability analysis appear in Alwi et al. (2012).

For each validation activity associated with the fault estimation and longitudinal C-NZ performance, the proposed scheme will be evaluated at the various flight conditions shown in Table 1 and 2 wherein 'MFW', 'MLW', 'MZFW' and 'MTOW' denote the maximum flight weight, the maximum landing weight, the maximum zero fuel weight and the maximum take-off weight, respectively. The acronyms 'VLS', 'VMO', 'MMO', 'ARS', 'AES' and 'VFE' represent the minimum selectable speed, the maximum operating speed, the maximum Mach operating speed, the automatic retraction speed for the high-lift system, the automatic extension speed for the high-lift system and the maximum speed when slat/flap (S/F) is extended, respectively. Specific numerical values for the various weights and speeds are not given in this paper due to industrial confidentiality requirements. In this paper, 228 various flight conditions which include 12 different mass cases and 19 different flight points (listed in Table–1 and 2) will be used for industrial Monte-Carlo V&V evaluation purposes in the presence of faults.

In this paper, the industrial V&V campaign results are generated using the RECONFIGURE Function Engineering Simulator (FES) developed by DEIMOS (Fernandez et al., 2015), which is a simulation software tool based on the

Table 1
Mass cases (MC) definition

Gross weight (t)	Centre Gravity (CG)(%)
MFW	Max forward CG
MFW	Medium CG
MFW	Max aft CG
(MLW+MZFW)/2	Max forward CG
(MLW+MZFW)/2	Medium CG
(MLW+MZFW)/2	Max aft CG
(MTOW+MLW)/2	Max forward CG
(MTOW+MLW)/2	Medium CG
(MTOW+MLW)/2	Max aft CG
MTOW	Max forward CG
MTOW	Medium CG
MTOW	Max aft CG

Table 2
Flight points (FP) definition

VCAS (kt)	Altitude h (ft)	S/F conf	Landing gear
VLS-5	Ceiling	0	Up
VMO/MMO	Ceiling	0	Up
VLS	30000	0	Up
VMO	30000	0	Up
VLS	15000	0	Up
250	15000	0	Up
VMO	15000	0	Up
(ARS+AES)/2-10	7500	1	Up
VFE	7500	1	Up
VLS	7500	1	Up
(ARS+AES)/2+10	7500	1	Up
VLS	5000	2	Up
VFE	5000	2	Up
VLS	2000	3	Up
VFE	2000	3	Up
VLS	1000	3	Down
VFE	1000	3	Down
VLS	1000	4	Down
VFE	1000	4	Down

MATLAB/SIMULINK modeling and simulation environment, specifically designed to support the industrial verification and benchmarking of the FDD/FTC algorithm prototypes designed by the partners in the RECONFIGURE project. The FES includes all the benchmark scenarios defined by AIRBUS with traditional Monte Carlo analysis, and provides an interface for a worst-case search tool for implementing advanced clearance methods (Goupil et al., 2015).

8.2.1 AIRBUS Technical Limitations and Constraints

On a large civil aircraft, the available computing capability of the Flight Control Computer (FCC) is relatively low, and proven reliable processors must be used for critical applications. Therefore, it is prohibited to use advanced processors capable of executing on-line optimisations or even wavelet or Fourier transforms in real time. In RECONFIGURE, to allow industry to evaluate the computational load of a particular design, each approach has been coded following the AIRBUS state of practice for FCC software coding – the SAO (AIRBUS software, Computer-Assisted Specification) library, which contains a set of graphical functional blocks (similar to SIMULINK blocks), allowing only a limited set of mathematical operations. An automatic generation tool then calculates the computational load and produces code to be implemented on the FCC. The computational load of the FTC scheme described in the earlier sections was deemed 'very low' when evaluated by AIRBUS, which is a positive feature of the design.

8.2.2 Monte Carlo campaign results in 'NZLAW-05'

The 'NZLAW-05' scenario has been used to evaluate the schemes' capability to maintain an ideal response to the load factor [3] demand across all flight conditions in the presence of a total loss of VCAS and AOA. The pilot excitations are shown in Fig. 6 wherein a sequence of positive and negative stick deflections are injected. In 'NZLAW-05', the 'AutoThrust' is engaged during the whole simulation. Note that due to AIRBUS industrial confidentiality constraints, the trajectories of the aircraft and details of the sensor faults cannot be shown in this paper.

It can be seen from Fig. 7 that $\|e_y\|$ is close to zero which demonstrates that sliding can be maintained despite the presence of faults in the AOA and VCAS measurements and various flight conditions. The fault reconstruction performance associated with VCAS faults and AOA faults are shown in Fig. 8 and Fig. 9, respectively. Figure. 8(a) shows the absolute value of the difference between the nominal VCAS and estimated VCAS, and Fig. 9(a) depicts the absolute value of the difference between the nominal AOA and the reconstructed AOA. Instead of showing the actual faults or system states, the fault reconstruction errors are depicted as percentages in this paper. Figure. 8(b) shows the absolute value of the normalized (percentage) VCAS fault reconstruction errors. The absolute value of the normalized (percentage) AOA fault reconstruction errors are shown in Fig. 9(b). It can be seen from Fig. 8 and Fig. 9 that the sliding mode observer scheme has the capability of estimating the scheduling parameter VCAS whilst reconstructing the AOA faults in all 228 operational conditions.

Note that in this test activity, only the absolute values of the differences associated with the crucial parameters of C-NZ control, (i.e. load factor n_z and the pitch rate q) between the nominal, the faulty (without any compensation) and the FTC cases are allowed to be shown due to industrial confidentiality restrictions. The absolute value of the differences in the n_z and q performance between the nominal and the faulty cases in the absence of the FTC scheme are shown in Fig. 10(a) and Fig. 11(a), respectively. The absolute value of the differences in the n_z and q performance between the nominal and the FTC cases are shown in Fig. 10(b) and Fig. 11(b), respectively. Clearly from Fig. 10 and 11, near nominal (fault-free) C-NZ performance can be retained using the FTC scheme in the presence of a simultaneous total loss of VCAS and AOA, throughout a large range of the flight envelope involving all the operational conditions defined in Table 1 and 2.

9 Conclusion

In this paper, an adaptive LPV sliding mode observer scheme has been proposed for sensor fault reconstruction despite erroneous scheduling parameter information. The algorithm has been developed based upon knowledge of the equivalent output error injection signal. The scheme attempts to estimate the erroneous scheduling parameters via an adaption scheme while simultaneously estimating the faults. Using the estimate of the faults, a virtual sensor can be created by compensating the measurements. The proposed scheme has been applied to a RECONFIGURE benchmark scenario that involves the total loss of the sensor measurement of AOA and the scheduling parameter VCAS. The industrial Monte Carlo campaign results show that the VCAS and AOA signals can be estimated accurately to achieve effective fault tolerant *C-NZ* performance.

References

Alwi, H., Edwards, C., 2008. Fault detection and fault-tolerant control of a civil aircraft using a sliding-mode-based scheme. IEEE Trans. Contr. Syst. Technol. 16(3), 499–510.

Alwi, H., Edwards, C., 2014. Robust fault reconstruction for linear parameter varying systems using sliding mode observers. Int J of Robust and nonlinear control 24, 1947–1968.

Alwi, H., Edwards, C., Menon, P., 2012. Sensor fault tolerant control using a robust LPV based sliding mode observer. In: IEEE CDC. pp. 1828–1833.

Alwi, H., Edwards, C., Tan, C. P., 2011. Fault Detection and Fault-Tolerant Control Using Sliding Modes. Springer.

Anstett, F., Millerioux, G., Bloch, G., 2009. Polytopic observer design for lpv systems based on minimal convex polytope finding. Journal of Algorithms & Computational Technology 3.

Chandra, K. P. B., Alwi, H., Edwards, C., 2016. Fault detection in uncertain LPV systems with imperfect scheduling parameter using sliding mode observers. European Journal of Control.

Daafouz, J., Bernussou, J., Geromel, J. C., 2008. On inexact LPV control design of continuous-time polytopic systems. IEEE Trans. Automat. Contr. 53(7), 1674–1678.

de Loza, A. F., Bejarano, F. J., Fridman, L., 2013. Unmatched uncertainties compensation based on high-order sliding mode observation. Int J of Robust and nonlinear control 23, 754–764.

Edwards, C., Spurgeon, S., Patton, R., 2000. Sliding mode observers for fault detection and isolation. Automatica 36, 541–553.

[3] The load factor is defined as the ratio of the lift of an aircraft to its weight.

Efimov, D., Edwards, C., Zolghadri, A., 2016. Enhancement of adaptive observer robustness applying sliding mode techniques. Automatica 72, 53–56.
Fernandez, V., Montano, J., Marcos, A., Rosa, P., Kerr, M., Dalbies, L., 2015. A tool for industrial verification and benchmarking of FDD/FTC designs. In: SAFEPROCESS'15. Paris, France, pp. 1006–1011.
Goupil, P., Boada-Bauxell, J., Marcos, A., Rosa, P., Kerr, M., Dalbies, L., 2015. An overview of the FP7 RECONFIGURE project: Industrial, scientific and technological objectives. In: SAFEPROCESS '15.
Hoffmann, C., Werner, H., 2015. A survey of linear parameter-varying control application validated by experiments or high-fidelity simulations. IEEE Trans. Contr. Syst. Technol. 23, 416–433.
Jiang, B., Staroswiecki, M., Cocquempot, V., 2004. Fault estimation in nonlinear uncertain systems using robust/sliding mode observers. IEE Proceedings - Control Theory and Applications 151, 29–37.
Khalil, H. K., 2000. Nonlinear Systems Third Edition. Pearson Education International Inc.
Löfberg, J., 2004. YALMIP : A toolbox for modeling and optimization in MATLAB. In: In Proceedings of the CACSD Conference. pp. 284–289.
Marcos, A., Balas, G. J., 2004. Development of linear-parameter-varying models for aircraft. AIAA Journal of Guidance, Control and Dynamics 27, 218–228.
Ossmann, D., Varga, A., 2015. Detection and identification of loss of efficiency faults of flight actuators. Int. J. Appl. Math. Comput. Sci. 25, 53–63.
Rotondo, D., Puig, V., Nejjari, F., J, R., 2015. A fault-hiding approach for the switching quasi-LPV fault-tolerant control of a four-wheeled omnidirectional mobile robot. IEEE Trans. Ind. Electron. 62, 3932–3944.
Sato, M., Peaucelle, D., 2013. Gain-scheduled output-feedback controllers using inexact scheduling parameters for continuous-time LPV systems. Automatica 49, 1019–1025.
Shtessel, Y., Edwards, C., Fridman, L., Levant, A., 2013. Sliding mode control and observation. Springer.
Tan, C., Edwards, C., 2002. Sliding mode observers for detection and reconstruction of sensor faults. Automatica 38(10), 1816–1821.
Utkin, V., 1992. Sliding modes in control and optimization. Springer.
Vanek, B., Edelmayer, A., Szabo, Z., Bokor, J., 2014. Bridging the gap between theory and practice in LPV fault detection for flight control actuators. Control Engineering Practice 31, 171–182.
Vanek, B., Szabo, Z., Edelmayer, A., Bokor, J., 2011. Geometric LPV fault detection filter design for commercial aircraft. In: AIAA Guidance, Navigation and Control Conference and Exhibit.
Varga, A., Ossmann, D., 2014. LPV model-based robust diagnosis of flight actuator faults. Control Engineering Practice 31, 135–147.
Yan, X., Edwards, C., 2008. Adaptive sliding-mode-observer-based fault reconstruction for nonlinear systems with parametric uncertainties. IEEE Trans. Ind. Electron. 55(11), 4029–4036.
Zhang, Q., 2002. Adaptive observer for multiple-input-multiple-output (MIMO) linear time-varying systems. IEEE Trans. Automat. Contr. 47(3), 525–529.

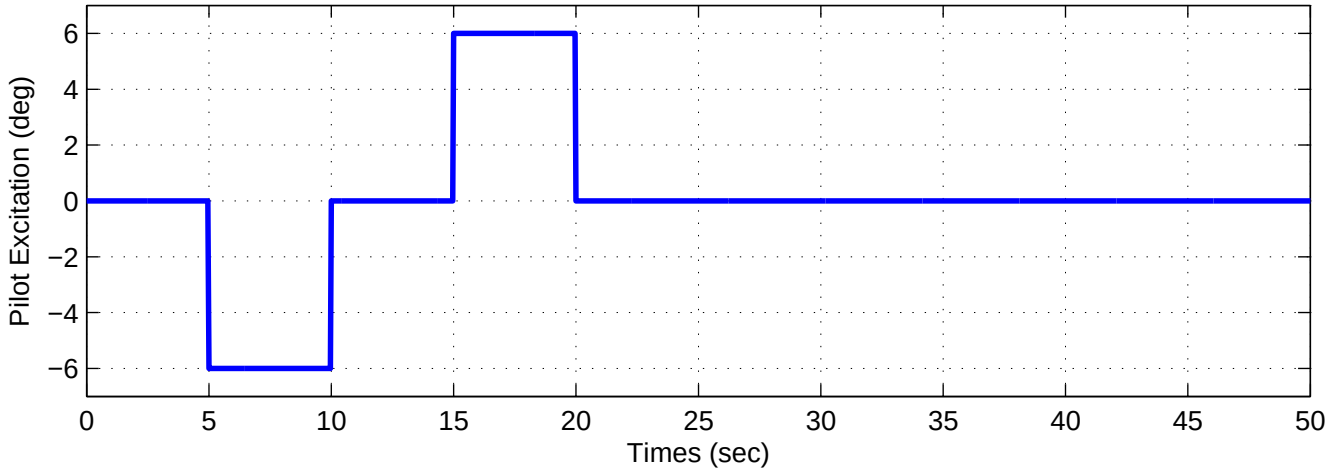

(a) Pilot Excitation

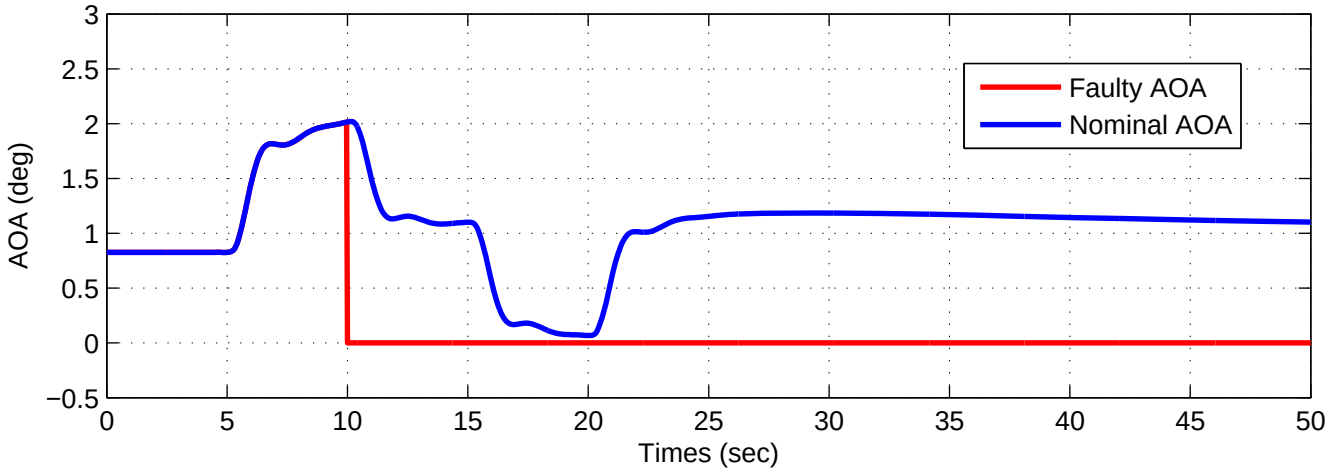

(b) Nominal AOA and faulty AOA

Fig. 3. Pilot excitation and AOA signals

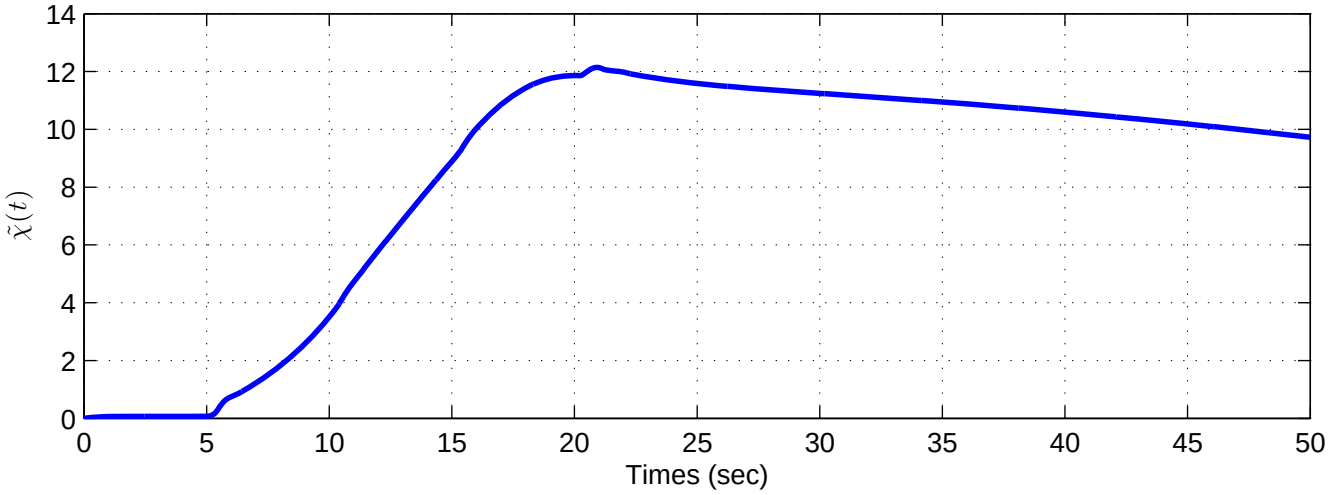

(a) $\tilde{\chi}(t)$

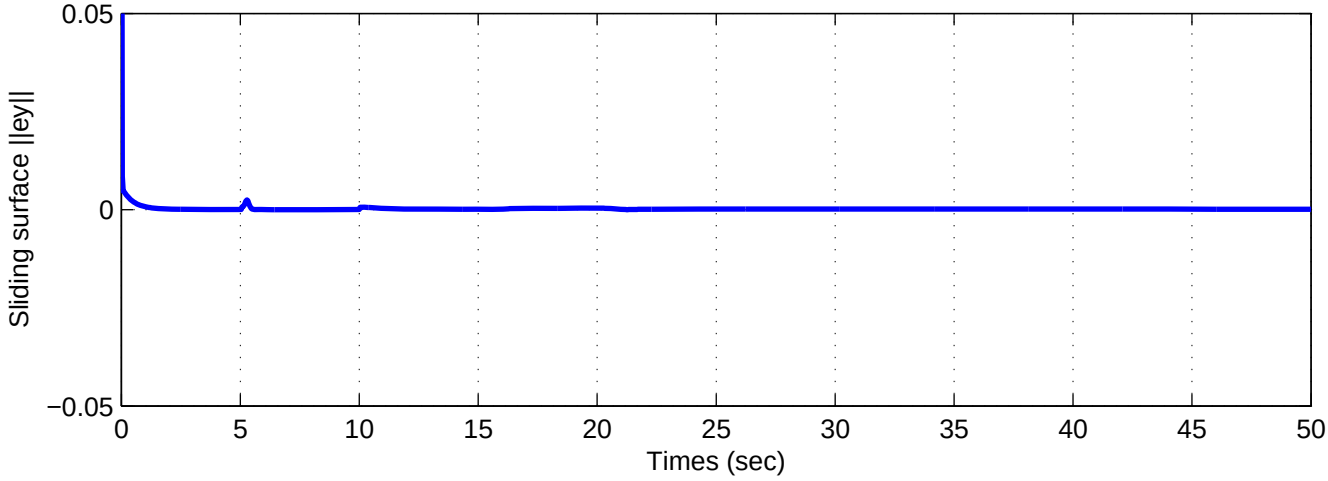

(b) Sliding surfaces $\|e_y\|$

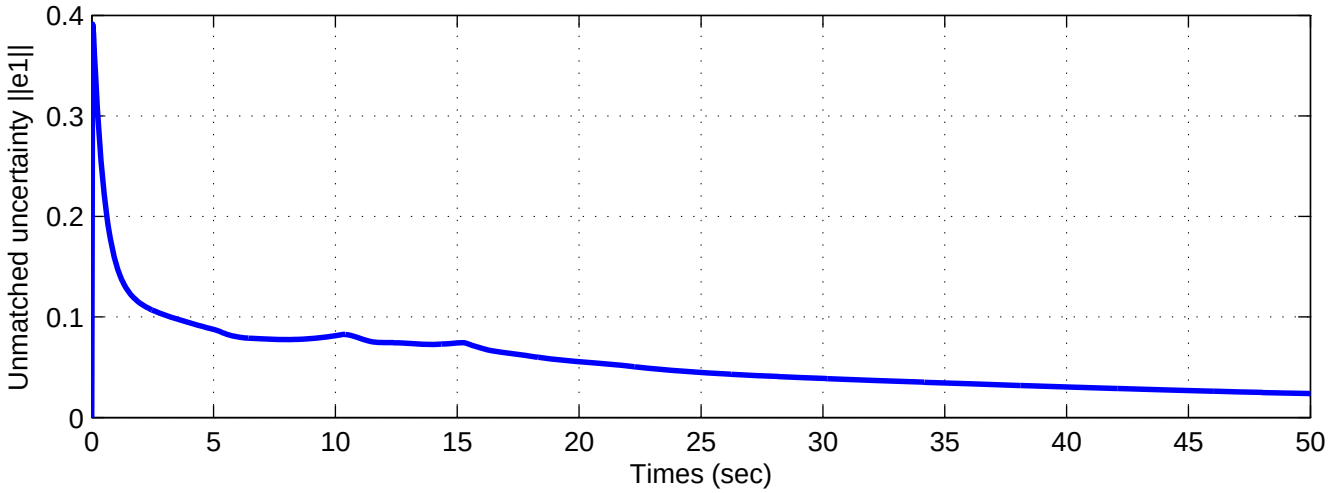

(c) Estimation error $\|e_1\|$

Fig. 4. $\tilde{\chi}(t)$, $\|e_y\|$ and $\|e_1\|$

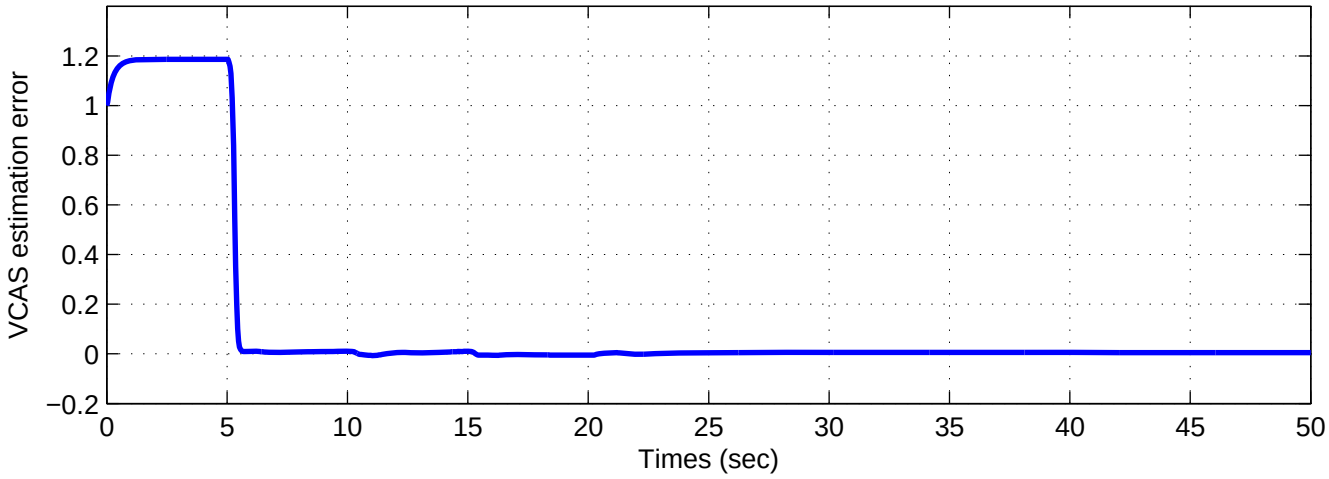

(a) VCAS estimation error $\tilde{\rho}_e$

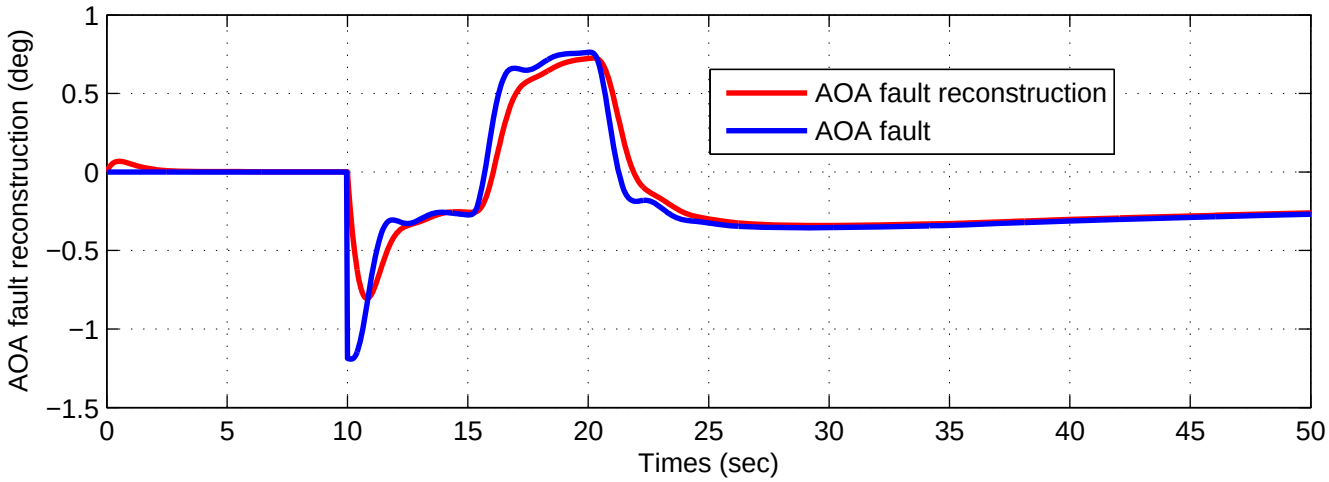

(b) AOA fault reconstruction

Fig. 5. $\tilde{\rho}_e$ and AOA fault reconstruction

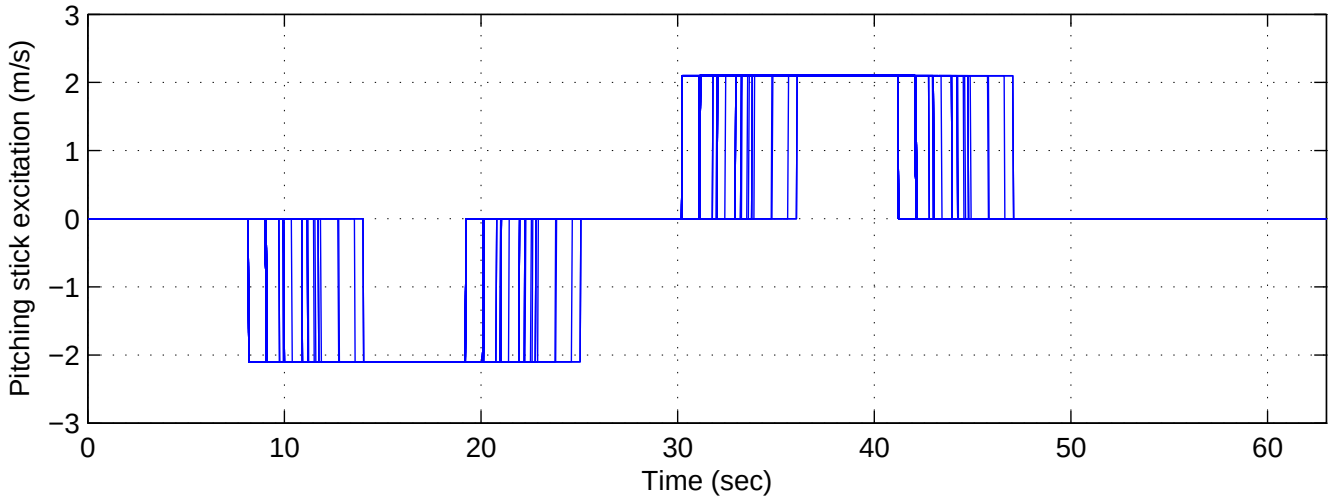

Fig. 6. Pitching stick excitations during 'NZLAW05'

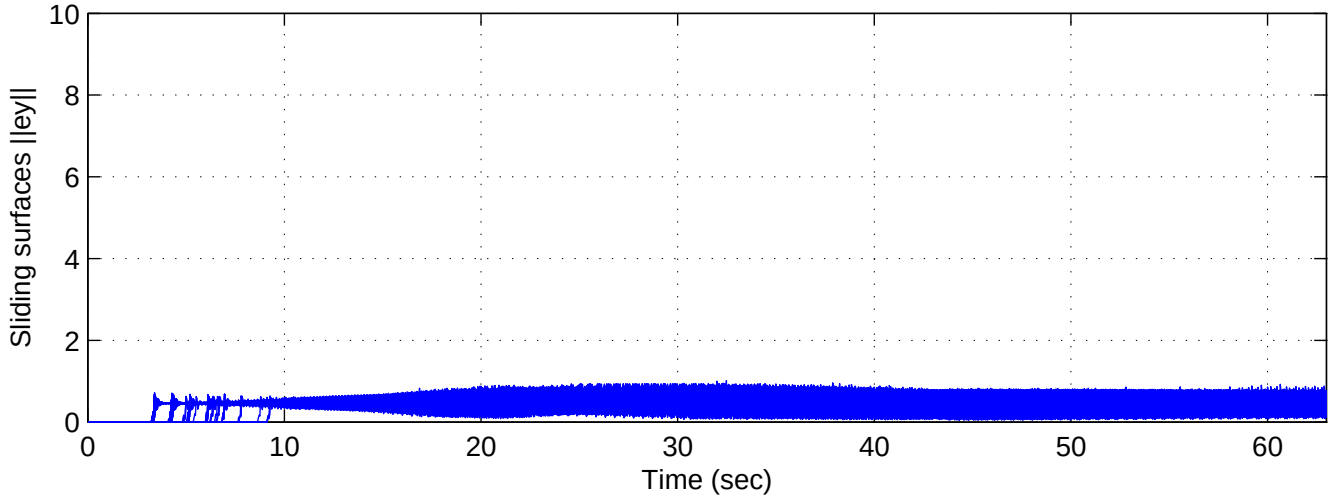

Fig. 7. Sliding surfaces $\|e_y\|$ during 'NZLAW05'

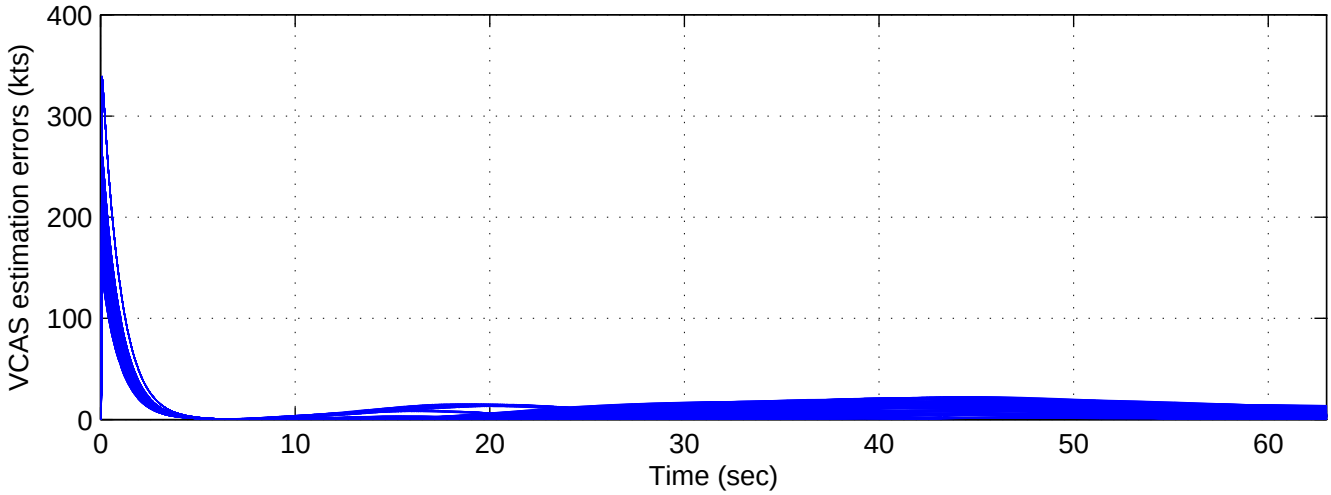

(a) The absolute values of the differences between the nominal VCAS and estimated VCAS

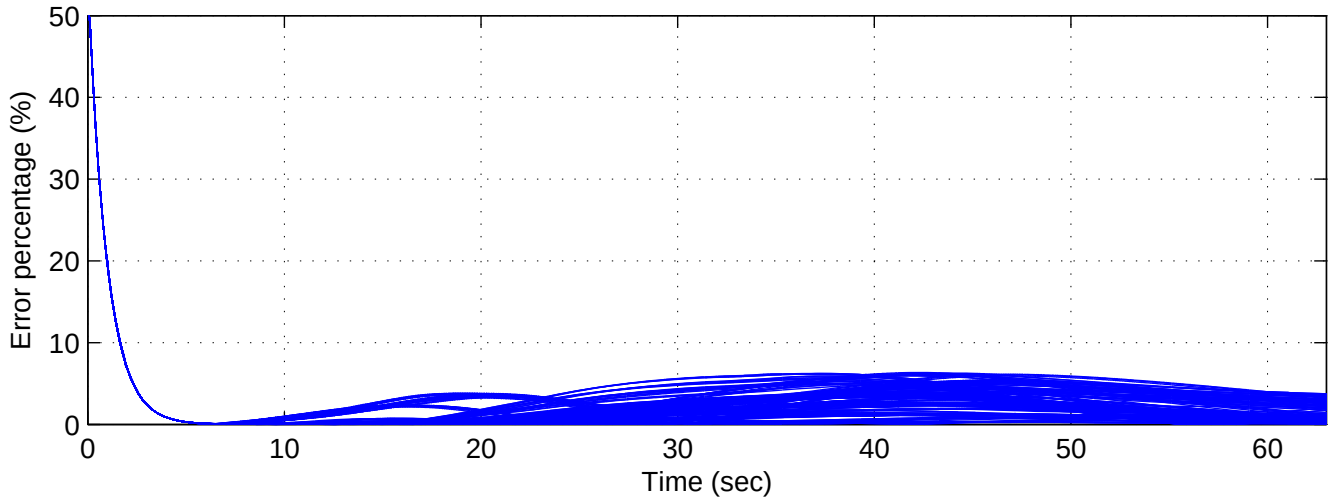

(b) VCAS reconstruction percentages

Fig. 8. VCAS reconstruction performance

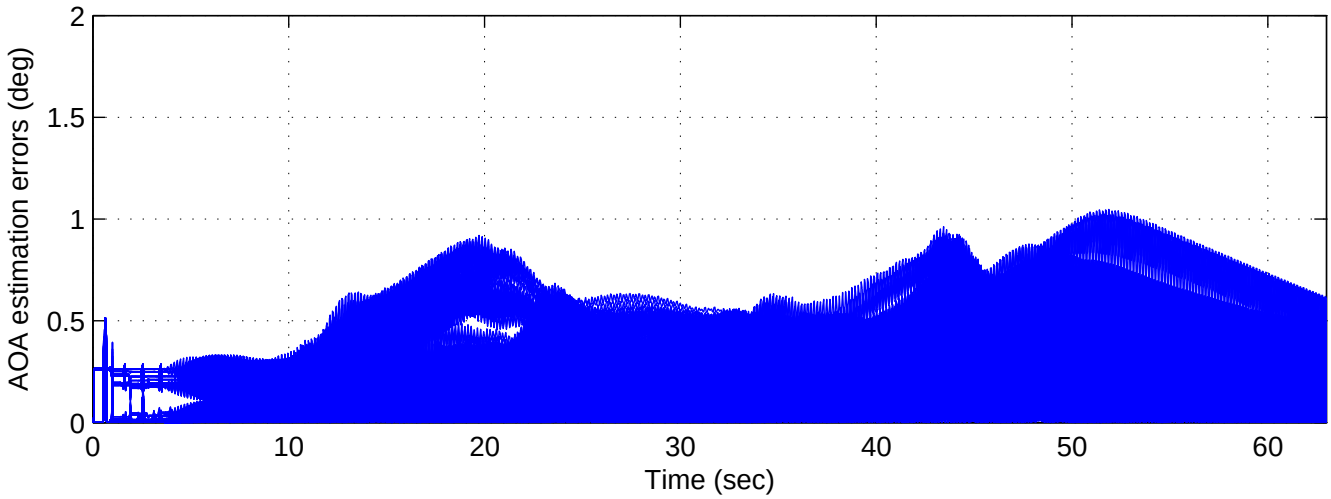

(a) The absolute values of the differences between the nominal AOA and estimated AOA

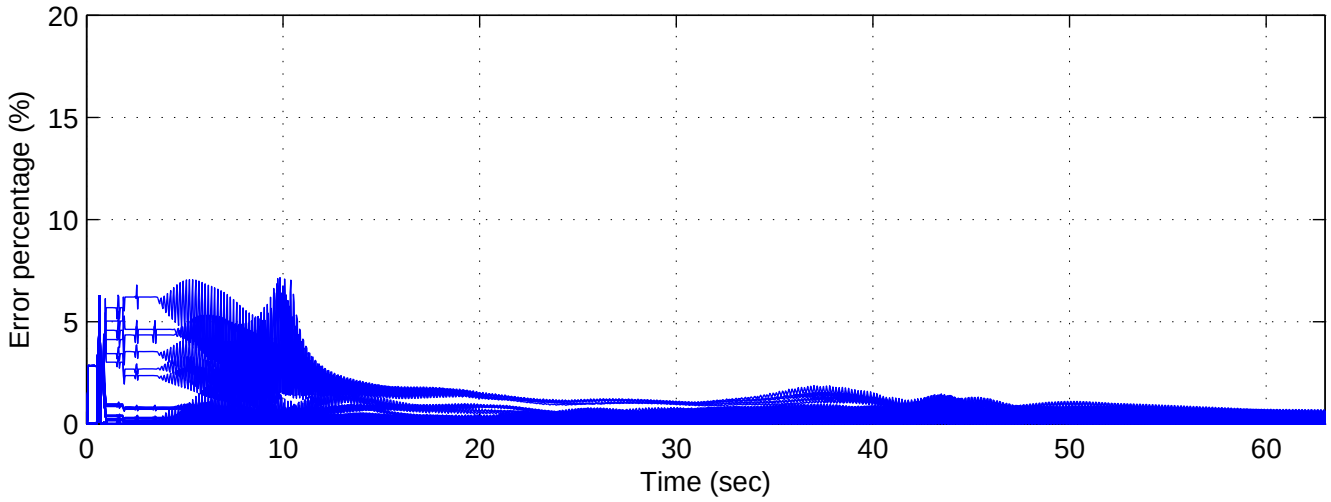

(b) AOA reconstruction percentages

Fig. 9. AOA reconstruction performance

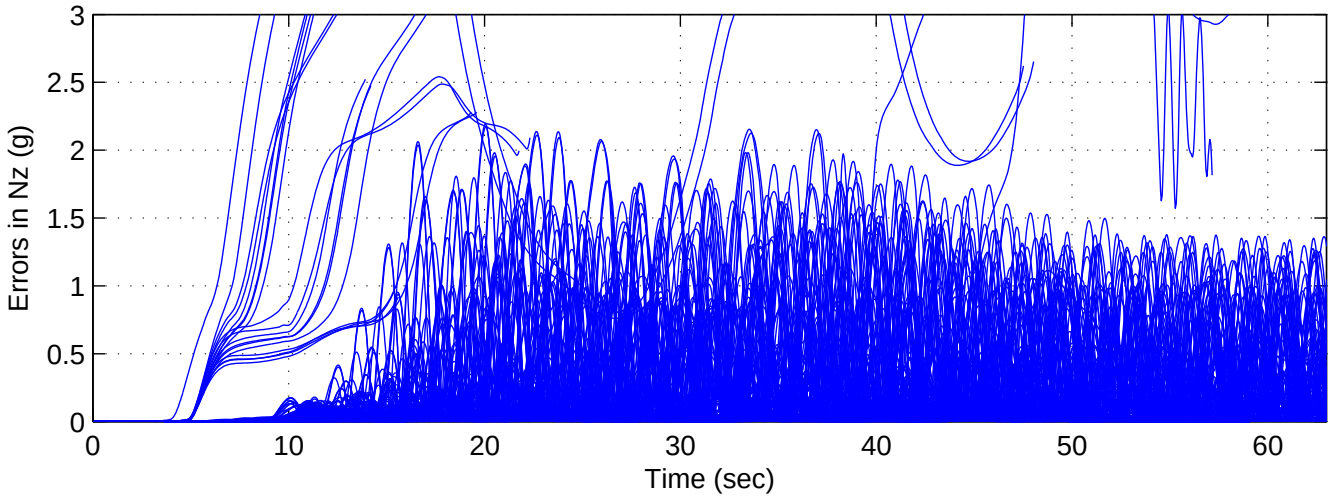

(a) The absolute values of the differences between the nominal and faulty cases

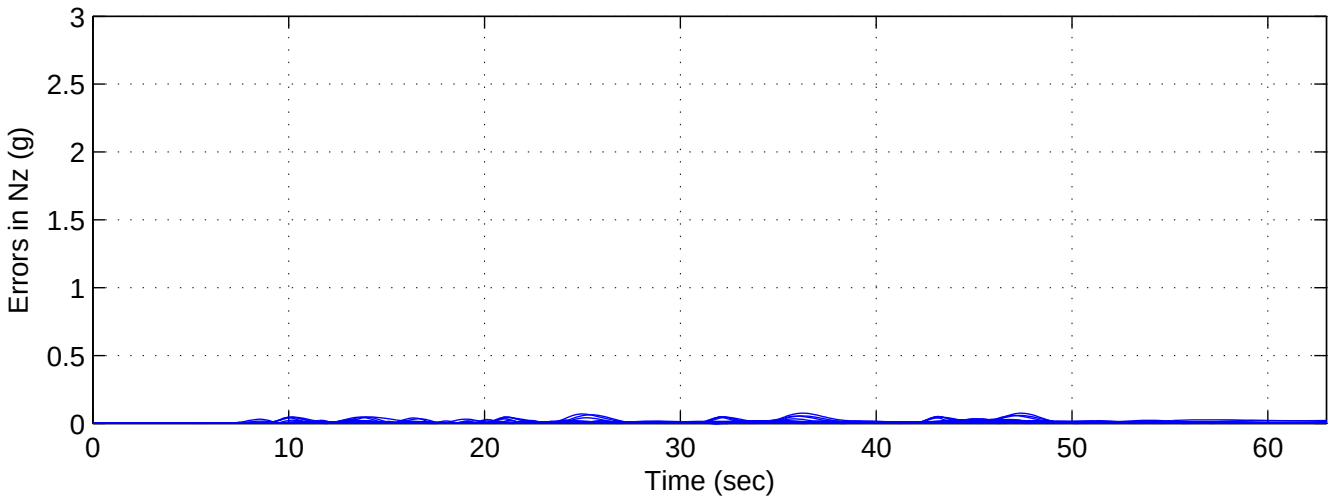

(b) The absolute values of the differences between the nominal and the FTC cases

Fig. 10. Load factor n_z performance in the presence of VCAS and AOA faults

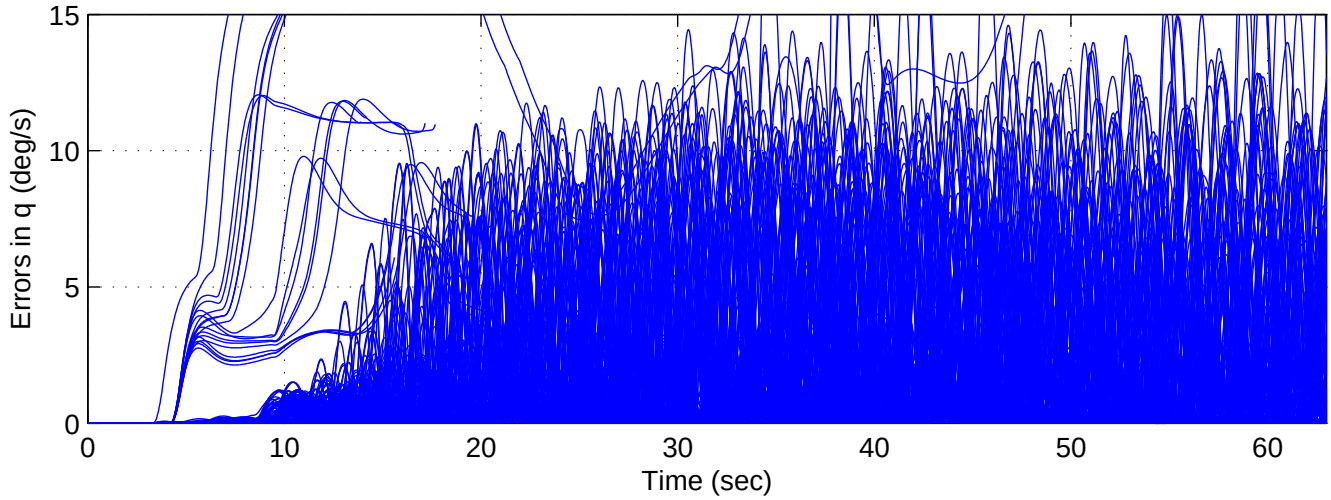

(a) The absolute values of the differences between the nominal and the faulty cases

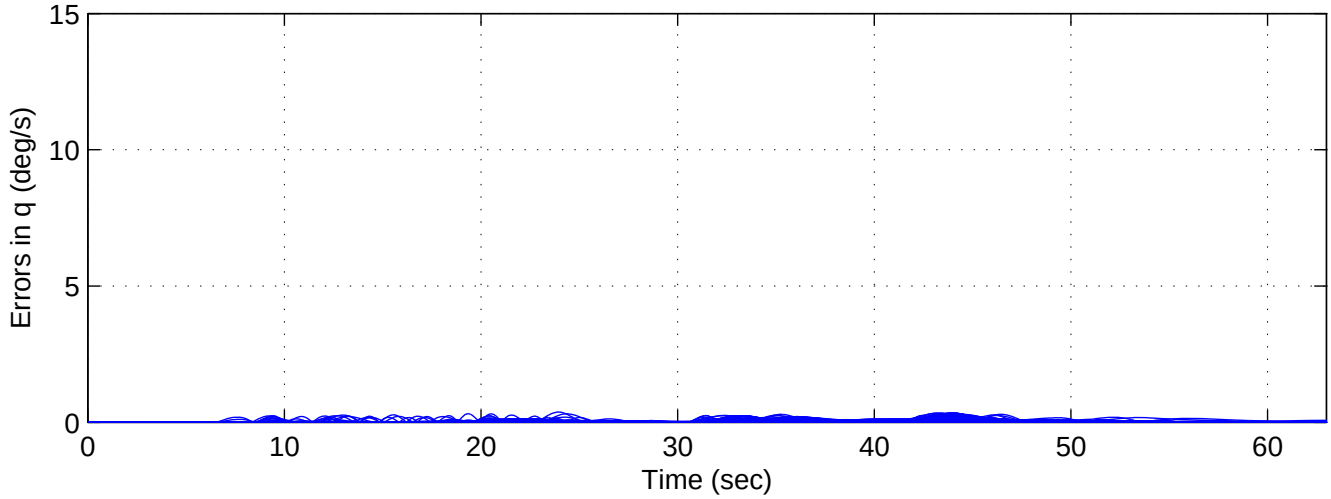

(b) The absolute values of the differences between the nominal and the FTC cases

Fig. 11. Pitch rate q performance in the presence of VCAS and AOA faults